Tectonics

RESEARCH ARTICLE
10.1029/2019TC005942

Crustal-Scale Sheath Folding at HP Conditions in an Exhumed Alpine Subduction Zone (Tauern Window, Eastern Alps)

Philip Groß[1], Mark R. Handy[1], Timm John[1], Gerhard Pestal[2], and Jan Pleuger[1]

[1]Freie Universität Berlin, Institute of Geological Sciences, Berlin, Deutschland, [2]Geologische Bundesanstalt, Wien, Österreich

Key Points:
- The central Tauern Window preserves a crustal-scale sheath fold that formed in the Alpine subduction zone in top-foreland shear
- The sheath fold was formed by passive amplification of a rift-inherited heterogeneity of the European margin
- Exhumation of sheath fold nappe from HP conditions was achieved at least partly by channel extrusion

Supporting Information:
- Supporting Information S1
- Figure S1
- Figure S2

Correspondence to:
P. Groß,
philip.gross@fu-berlin.de

Citation:
Groß, P., Handy, M. R., John, T., Pestal, G., & Pleuger, J. (2020). Crustal-scale sheath folding at HP conditions in an exhumed Alpine subduction zone (Tauern Window, Eastern Alps). *Tectonics*, *39*, e2019TC005942. https://doi.org/10.1029/2019TC005942

Received 23 OCT 2019
Accepted 4 FEB 2020
Accepted article online 15 FEB 2020

Abstract We investigate a well-preserved paleo subduction channel that preserves a coherent part of the European continental margin exposed in the central Tauern Window (Eastern Alps), with the aim of testing models of sheath fold nappe formation and exhumation. The subduction zone was active during Paleogene convergence of the European and Adriatic plates, after closure of the Alpine Tethyan ocean. New cross sections and structural data together with new petrological data document a recumbent, tens of kilometers-scale sheath fold in the center of the Tauern Window that formed during pervasive top-foreland shear while subducted at high-pressure (HP) conditions (~2.0 GPa, 500 °C) close to maximum burial depth. The fold comprises an isoclinally folded thrust that transported relicts of the former Alpine Tethys onto a distal part of the former European continental margin. The passive margin stratigraphy is still well preserved in the fold and highlights the special character of this segment of the European continental margin. We argue that this segment formed a promontory to the margin, which was inherited from Mesozoic rifting. In accordance with classical sheath fold theory, this promontory may have acted as an initial structural perturbation to nucleate a fold that was passively amplified to a sheath fold during top-foreland shear in the subduction zone. The fold was at least partly exhumed and juxtaposed with the surrounding lower pressure units by opposing top-hinterland and top-foreland shear zones above and below, respectively, that is, in the sense of a nappe fold formed during channel-extrusion exhumation.

1. Introduction

Exhuming continental lithosphere from great depths has posed a geodynamic problem ever since the discovery of high-pressure (HP) and ultra-high pressure (UHP) mineral assemblages in continental units in the heart of mountain belts (e.g., Chopin, 1984; Okay et al., 1989). These units, henceforth referred to as HP units, form in the former lower plate of orogens prior to, or at the beginning of, continental collision. The basic challenge has been to determine how crustal units that densified during prograde subduction metamorphism (e.g., Agard et al., 2009; Bousquet et al., 1997) have risen within the orogen and were emplaced next to, and in some cases between, less dense units during crustal thickening. Unfortunately, most HP units have been strongly overprinted during and after exhumation, which has eliminated most, if not all, structures related to subduction and even to exhumation from HP and UHP conditions (e.g., Beltrando et al., 2010; Jolivet et al., 2003; Pleuger & Podladchikov, 2014).

This challenge has been addressed mostly by numerical modelers, who have attempted to fill the information gap with models using various dynamic boundary conditions (reviews by Agard et al., 2018; Hacker et al., 2013; Warren, 2013). One end-member proposal, here termed the "wedge model" after the critical wedge theory of Chapple (1978) and Dahlen et al. (1984), involves the progressive exhumation of deeply subducted nappes from the base of orogenic wedges due to tectonic and erosional unroofing of the overlying nappe stack (Beaumont et al., 1994; Platt, 1986). Thrusting in the wedge-shaped nappe stack is proposed to be "in sequence," that is, to propagate toward the foreland, while the nappe stack unroofs to maintain a force balance between the dipping wedge base, the tapered wedge surface, and the nappe stack itself. Unroofing may be accelerated by uplift of the entire wedge due to removal of negatively buoyant lithospheric mantle from the base of the orogen, either by convective delamination (Houseman et al., 1981) or by tearing and breakoff of a lithospheric slab (Davies & von Blanckenburg, 1995). A contrasting model, here termed the "channel" model, involves subducted crustal fragments rising as buoyant bodies along a narrow channel at

the top of a descending lithospheric slab (Chemenda et al., 1995; see also Burov et al., 2001). In the case of negatively buoyant HP rock bodies, this ascent may be facilitated by downward narrowing of the channel, which would forcibly extrude the subducted bodies upward between a thrust and normal fault located, respectively, in the footwall and hanging wall of these bodies (Mancktelow, 1995; Vannay & Grasemann, 2001). Yet another way to solve the dilemma of HP rocks within orogens has been to posit that the pressure values recorded in HP units by petrology reflect dynamic pressure rather than lithostatic pressure, P (e.g., Mancktelow, 1993, 1995, 2008; Moulas et al., 2013; Petrini & Podladchikov, 2000; Rutland, 1965). Dynamic pressure, sometimes called tectonic overpressure or underpressure (depending on the sign), is the difference between mean stress (i.e., $(\sigma_1 + \sigma_3)/2$) and the lithostatic pressure. If one assumes that mean stress can be equated with thermodynamic pressure, then the pressure values obtained by applying phase petrology to HP rocks in compressional settings correspond to a shallower depth than obtained by assuming the standard geobaric relationship of $P = \rho g z$, where ρ is rock density, g is the acceleration of gravity, and z is depth (Gerya, 2015; Moulas et al., 2013; Schenker et al., 2015). Though dynamic pressure mitigates the problem of exhumation by reducing the depth of subduction, the assumption that mean stress can be equated with thermodynamic pressure is a proposition that remains highly controversial (e.g., Tajčmanová et al., 2014; Wheeler, 2014).

Variants of these end-member hypotheses have been applied to the European Alps (Figure 1, inset; Bauville & Schmalholz, 2015; Escher & Beaumont, 1997; Schmid et al., 1996), where Alpine HP and UHP metamorphism affected not only oceanic units but also continental units derived from the margins of both the European and Adriatic plates (Bousquet et al., 2012; Oberhänsli et al., 2004; maps and references therein). These continental units individuated already during Early Mesozoic rifting and spreading of the Alpine Tethyan ocean (e.g., Froitzheim & Manatschal, 1996). The SE to NW younging of the HP ages in the imbricated oceanic and continental units is interpreted to indicate that these units were subducted and exhumed in a piecemeal fashion during retreating subduction of the European Plate beneath the Adriatic Plate (e.g., Babist et al., 2006; Gebauer, 1999; Handy et al., 2010). The exposure of subduction and exhumation structures is exceptionally good in the Tauern Window of the Eastern Alps (Figure 1), where glacially carved mountains with bare outcrop surfaces and a relief of up to 3,000 m afford a three-dimensional view of the Adria-Europe suture zone.

In this paper, we present the first clear kinematic and petrological evidence for the formation of a crustal-scale, recumbent sheath fold during Alpine subduction in Paleogene time. We show that this sheath fold —beautifully exposed in the central Tauern Window—contains an isoclinally folded thrust responsible for the emplacement of ocean crust onto fragments of the distal European continental margin. This folded nappe complex was then exhumed as a coherent unit during shearing under blueschist-facies to greenschist-facies retrograde conditions. We then discuss the tectonometamorphic conditions that were conducive for forming the sheath fold and for preserving the original stratigraphy of the continental margin within that fold. The tectonometamorphic evolution of this fold nappe is then used to test the aforementioned ideas on the exhumation of deeply buried crust, including the orogenic wedge and channel-extrusion models.

2. Geological Setting

2.1. General Overview

The tectonic units investigated in this paper (Figure 2) comprise thrust sheets of oceanic lithosphere derived from the Alpine Tethyan ocean (e.g., Schmid et al., 2004), as well as folded and sheared thrust sheets of the distal European continental margin (Kurz et al., 1998). Following Schmid et al. (2013), we refer to these, respectively, as the Glockner nappe system (oceanic origin) and the Modereck nappe system (continental origin). The former is part of the Penninic nappes and the latter of the Sub-Penninic nappes. Parts of the Glockner nappe system contain HP mineral assemblages (e.g., Cornelius & Clar, 1934a; Dachs & Proyer, 2001; Frank et al., 1987), indicating that at least some of the oceanic units were subducted to great depth and exhumed during the Alpine orogeny. As shown by Proyer et al. (1999) and Dachs and Proyer (2001) and documented below, the continental Modereck nappe system was also affected by the same HP event.

The overlying Austroalpine nappes forming the perimeter of the Tauern Window are derived from the Adriatic Plate (Figure 1), whereas the underlying units in the core of the Tauern Window derive from the

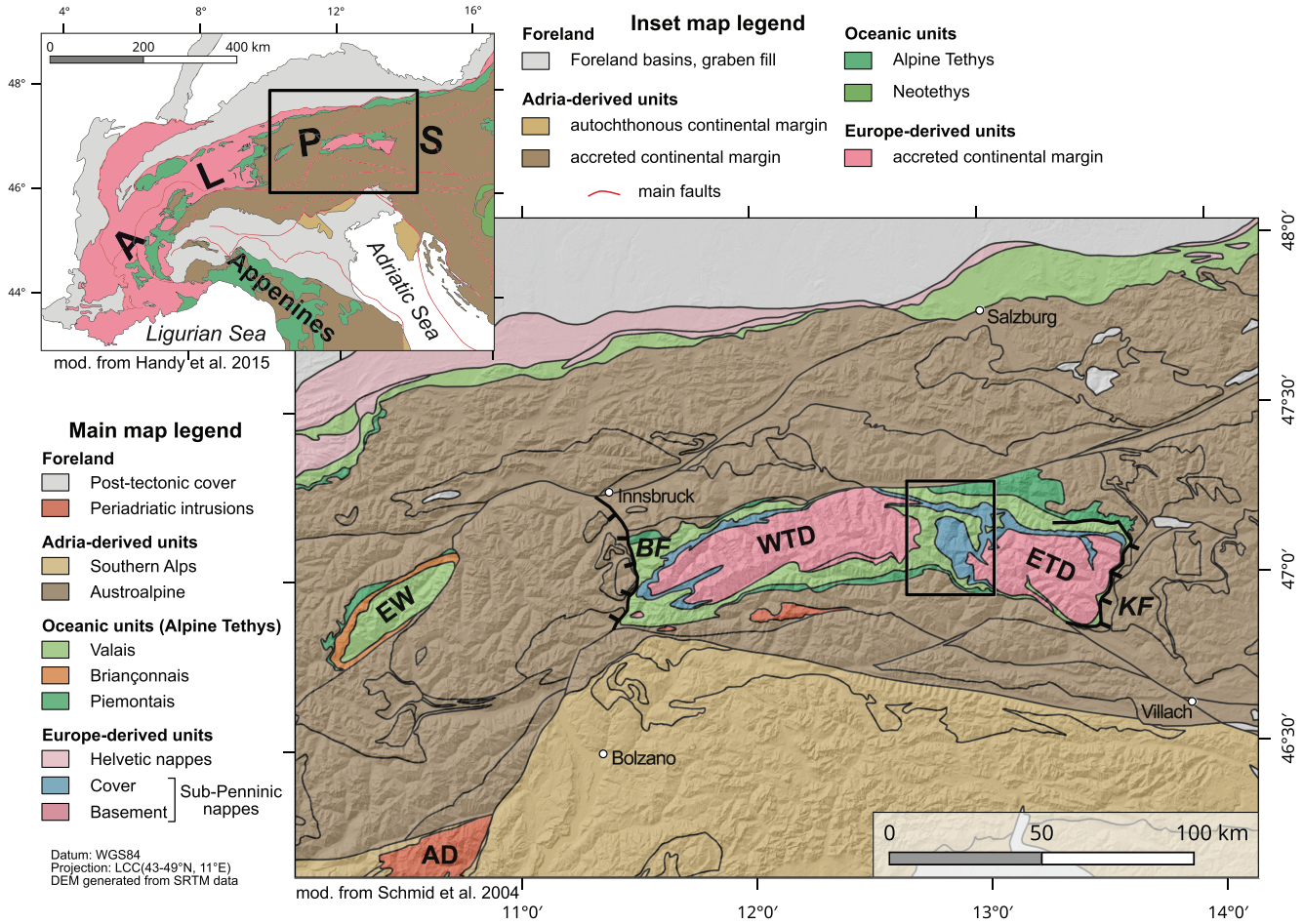

Figure 1. Tectonic map of the Eastern Alps and Tauern Window with the Western Tauern Dome (WTD) and Eastern Tauern Dome (ETD). Map modified from Schmid et al. (2004, 2013); inset map of the Alps modified from Handy et al. (2015). Black rectangle outlines the study area and location of the tectonic map in Figure 2. AD = Adamello Pluton, EW = Engadin Window, BF = Brenner Fault, KF = Katschberg Fault.

European continental margin (Lammerer, 1986; Schmid et al., 2013). All units and nappe contacts, including the aforementioned HP assemblages in the Penninic nappes, were overprinted by a Barrow-type, high T/P metamorphic event, the so-called Tauernkristallization (Sander, 1914; see also Dachs et al., 2005; Droop, 1985; Hoinkes et al., 1999) in late Oligocene time (e.g., Cliff et al., 1985; Favaro et al., 2015; Höck & Miller, 1980). This event varies in metamorphic grade from peak amphibolite facies conditions in the two basement subdomes at either end of the Tauern Window to greenschist facies in the central Tauern Window (e.g., Droop, 1985; Hoernes & Friedrichsen, 1974; Scharf, Handy, Ziemann, & Schmid, 2013).

Here, we deal specifically with the internal structure of the Penninic and upper part of the Subpenninic nappes. The aforementioned Glockner and Modereck nappe systems are separated by a thrust that is isoclinally folded, with the Modereck nappe system forming the core of an isoclinal fold (Figure 1). Below, we show that this fold, first described by Frank (1965, 1969) and later by Alber (1974) as the Seidlwinkl Fold, is a crustal-scale isoclinal sheath fold nappe that formed under HP conditions in the Alpine subduction zone. The primary geometry of the Seidlwinkl Fold is complicated by folding around a NW-SE trending dome, the Sonnblick Dome, in the eastern Tauern Window (Figure 1). The eastern limb of this dome preserves the inverted limb of the Seidlwinkl Fold; this inverted limb lies above the roof thrust of an imbricate stack of Subpenninic basement nappes, the Venediger nappe complex (Figure 1).

Schmid et al. (2013) used superposed map-scale structures to propose the following succession of tectonometamorphic events for the Tauern Window: D1—thrusting of the Austroalpine nappes onto the Matrei Zone (southern part of Alpine Tethys); D2—thrusting of the Glockner nappe system (northern part of Alpine

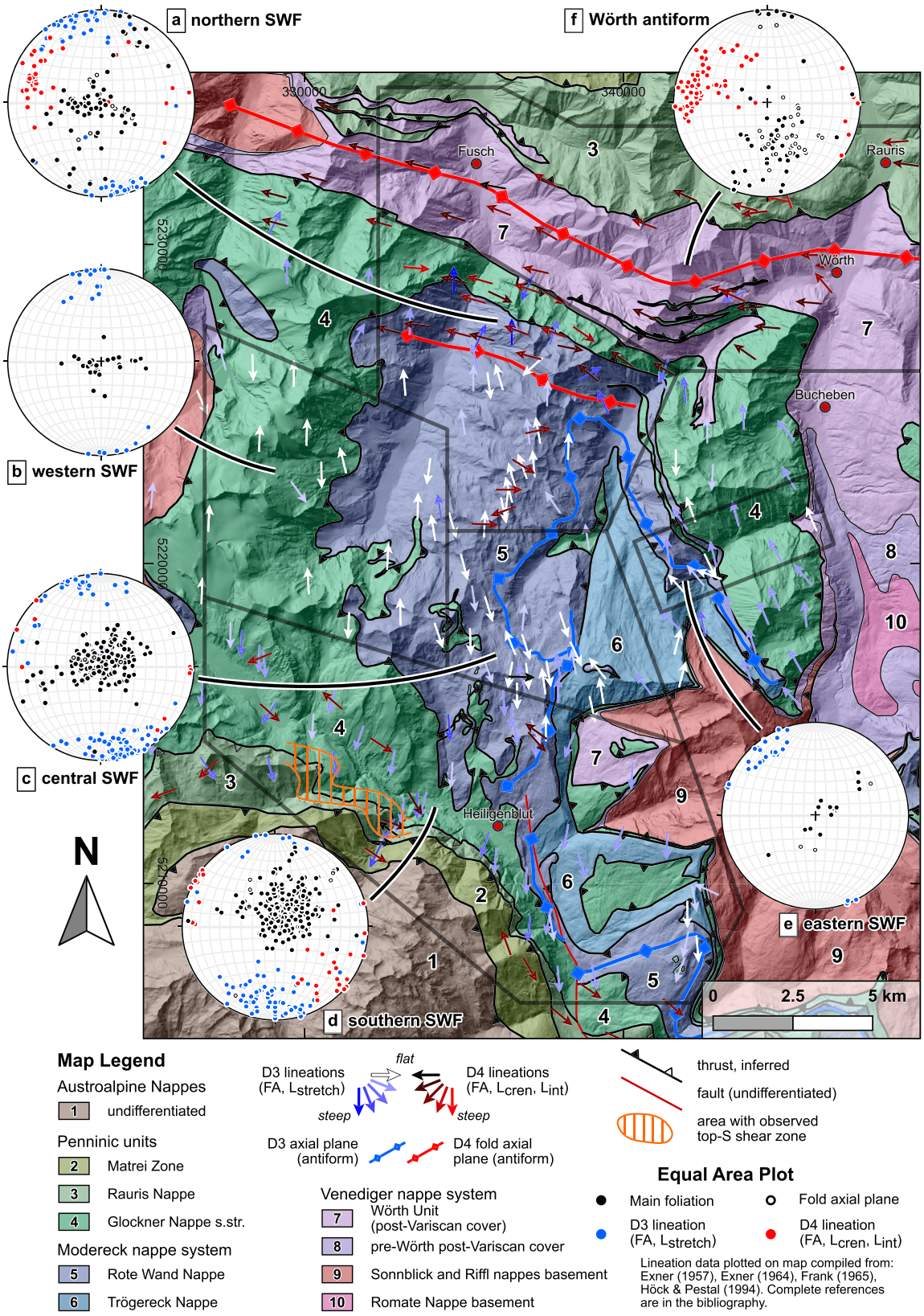

Figure 2. Tectonic map of the central Tauern Window with lower hemisphere equal area plots showing poles to the main S3 schistosity, D3 and D4 lineations. Data plotted on the map were compiled from own field measurements and C. Exner (1957), C. Exner (1964), Frank (1965), and Höck and Pestal (1994). Structural data in the equal area plots are exclusively from own field observations. SWF = Seidlwinkl sheath fold nappe.

Tethys) onto the Modereck nappe system (distal European margin), forming a composite ocean-on-continent nappe that reached HP conditions within the Alpine subduction zone; D3—isoclinal folding of this composite HP nappe (the Seidlwinkl fold nappe) and exhumation onto the European margin above a basal thrust; D4—imbrication of this margin below the original basal thrust to form a duplex of Subpenninic nappes, then subsequent "Tauernkristallisation" Barrovian metamorphism; D5—doming and orogen-parallel stretching accommodated along oppositely WSW-dipping and SE-dipping, low-angle normal faults at either end of the Tauern Window, respectively, the Brenner and Katschberg Normal Faults (Figure 1). The formation of the Tauern Window itself is attributed to a combination of tectonic and erosional unroofing during D5 in response to northward indentation of the Adriatic Plate into the warm and thick Alpine orogenic crust (e.g., Favaro et al., 2017; Ratschbacher et al., 1991; Rosenberg et al., 2007).

In the following, we adopt the numbering above to identify the relative age of the different structures in the central Tauern Window. However, linking the D2 juxtaposition of the Glockner and Modereck nappe systems, as well as the D3 Seidlwinkl folding to the HP metamorphic event in the central Tauern Window, remains an elusive endeavor. Determining this link is crucial to understanding how such folds nucleate and grow, as well as when they form in relation to subduction and exhumation. Metabasites from the Glockner Nappe (Figure 2) yield peak pressures of up to ~1.7 GPa at 570 °C (Dachs & Proyer, 2001; Proyer et al., 1999). These authors interpreted the metabasites as exotic blocks in a meta-sedimentary matrix that never experienced such high pressure. However, other studies indicate that HP mineral assemblages are widespread in the Penninic units of the central Tauern Window and the continentally derived metasediments of the Modereck nappe system (e.g., Dachs & Proyer, 2001; Frank et al., 1987; Proyer et al., 1999; Schmidt et al., 2014). One of our goals is therefore to reconstruct the tectonometamorphic evolution of HP rocks in the central Tauern Window, with special emphasis on the highly deformed Mesozoic metasediments that form the cover of the continentally derived Modereck nappe system.

2.2. Lithostratigraphic Units of the Central Tauern Window

The lithostratigraphy of the nappes in the central Tauern Window established in previous work (e.g., Kurz et al., 1998; Pestal & Hellerschmidt-Alber, 2011; Schmid et al., 2013) is central to our map compilation, cross-section construction, and thermobarometry in the following chapters. The two structural domes at either end of the Tauern Window (ETD and WTD in Figure 1) are separated by a structural depression preserving the Seidlwinkl sheath fold that comprises the folded Modereck nappe system and Glockner Nappe (boxed area in Figure 1). The lowest tectonic units (Venediger nappe system) exposed in the cores of the domes consist of late-Variscan granitoids ("Zentralgneise") that intruded into pre-Variscan European metamorphic basement ("Altes Dach"). These basement rocks are discordantly overlain by Permo-Triassic (Wustkogel Formation, meta-arkose and meta-sandstone) to presumably Cretaceous metasediments (graphitic phyllites, named the Wörth Unit by W. Frank, personal communication August 16, 2017). The Venediger nappe system lies structurally below the Eclogite Zone and Modereck nappe system, which represent the most distal part of the former European margin (Kurz et al., 1998; Schmid et al., 2013). In the study area, the Modereck nappe system comprises two nappes: the (lower) Trögereck (Pestal & Hellerschmidt-Alber, 2011; after C. Exner, 1964) and (upper) Rote Wand nappes. The latter is sometimes referred to as the Seidlwinkl Nappe (Pestal & Hellerschmidt-Alber, 2011) or Rote Wand-Modereck Nappe (Kurz et al., 1998), but we avoid this double name and simply use the term Rote Wand Nappe to prevent any further confusion with the Seidlwinkl fold nappe (above) and Seidlwinkl Formation (below). The Rote Wand Nappe comprises a lamella of gneiss and micaschist overlain by a complete stratigraphic sequence typical of the European continental margin (Kurz et al., 1998). The base of this sequence is Permo-Triassic meta-arkose (Wustkogel Formation, Pestal, 2008) overlain by mid-Triassic lagoonal carbonates and evaporites (Seidlwinkl Formation) and upper Triassic terrestrial pelites and quartzites (Piffkar and Schwarzkopf formations, Pestal, 2008). The stratigraphy of the Rote Wand Nappe is topped by graphite-bearing carbonatic schist and quartzite of the Brennkogel Formation (Frasl & Frank, 1966) of presumably lower Cretaceous age (Schmid et al., 2013). These rocks are interpreted to have been deposited on a distal part of the European margin and were laterally transitional to the "Bündnerschiefer" calc-schists of the adjacent Alpine Tethys (Schmid et al., 2013). The Trögereck Nappe consists of a less well-stratified succession of similar rocks (granitic gneiss, arkosic gneiss, Bündnerschiefer-type calcschist, and marble; Pestal & Hellerschmidt-Alber, 2011) and also lenses of metabasite (exposed, e.g., in the area of the Hinteres Modereck summit; see Figure S1) and may well represent a

former syn-rift sedimentary sequence at the European continental margin. In our view, its lithological assemblage is akin to that of the Eclogite Zone further in the west, at the southern rim of the Tauern Window. As a working hypothesis, we therefore consider these two tectonic units to be lateral equivalents.

In most of the Tauern Window, the Glockner nappe system lies on top of the Modereck nappe system. The Glockner nappe system consists of serpentinite bodies at its base overlain by large volumes of calcareous micaschist (Bündnerschiefer) and layers of metabasite (prasinite and relict eclogite) derived from the northern part of Alpine Tethys. Our observations support the proposal by Pestal and Hellerschmidt-Alber (2011) that the Glockner nappe system comprises two nappes: a lower one with eclogite-facies parageneses (Glockner Nappe s. str.) and an upper one with blueschist-facies to greenschist-facies parageneses (Rauris Nappe). The Glockner nappe system is overlain by the Matrei Zone comprising rocks that originate from the older (Jurassic) and originally more southern Piemont part of Alpine Tethys (Handy et al., 2010). We note that the contact between the Rauris part of the Glockner nappe system and the overlying Matrei Zone is often gradational (e.g., Frisch et al., 1987), rendering a clear delineation of the thrust contact between these units difficult. However, they can nevertheless be distinguished where olistoliths or tectonic slivers of Austroalpine rocks are present, which is diagnostic of the Matrei Zone near the originally adjacent distal Adriatic margin (e.g., Frisch et al., 1987). The Matrei Zone is in turn overlain by Austroalpine units.

3. Structures

In this section, we describe the microscale to outcrop-scale structures and their orientations, as well as their relationship to crustal-scale structures as shown in a new tectonic map (Figure 2), a lithological map (Figure S1 in the supporting information), and a series of cross sections (Figures 3 and S2). Higher resolution versions of the map and all sections are found in the supporting information together with the underlying data, information on sources, map compilation, and cross-section construction.

Structures and their kinematics in the central part of the Tauern Window are directly related to the D1 to D5 regional deformation phases outlined above and previously defined by Kurz et al. (2008) and Schmid et al. (2013) based on their interpretation of map-scale structures.

D1 is marked by the thrust of the Austroalpine nappes onto the oceanic Matrei Zone. D2 is represented by two subduction-related thrusts: (1) the originally intraoceanic thrust of the Matrei Zone (southern part of Alpine Tethys) onto the Glockner nappe system (northern part of Alpine Tethys) and (2) the thrust of the Glockner nappe system onto the Modereck nappe system (distal European margin). This later thrust therefore marks the onset of continental subduction. Additionally, we consider the fault between the Rauris Nappe and the Glockner Nappe s. str. as a D2 thrust along which the Glockner Nappe s. str. was subducted.

On the outcrop scale, D2 in the Glockner and Rote Wand nappes is marked by a relict schistosity, S2, defined by HP mineral parageneses. S2 is parallel to the older compositional layering that we interpret as the original bedding. Both of these foliations are parallel to the D2 thrusts (Figures 3 and S2). S2 is preserved in the hinges of D3 isoclinal folds (Figure 4a) and in garnet inclusions, for example, lawsonite pseudomorphs and glaucophane (Figure 4c).

D3 structures predominate in the study area, more than in any other part of the Tauern Window where D4 and D5 deformations completely transpose older structures. The most obvious D3 structure is the spectacular F3 Seidlwinkl fold nappe, which isoclinally folds the D2 thrust separating the Glockner and Rote Wand nappes, with the latter forming the core of the fold. Its axial plane foliation, S3, is the main foliation in the area. The fold has an arcuate axial trace in map view (Figure 2) that is diagnostic of sheath folds (Cobbold & Quinquis, 1980). Indeed, our cross sections confirm this geometry: The D3 sheath fold roots in the south (Figure A2, profile H) and closes toward east and west (Figure 3, profile B; Figure A2, profiles B–G) as well as to the north (Figure 3, profile A; Figure A2, profile A), which results in a typical sheath fold geometry (Figure 4d) and is also consistent with the observed kinematics and microstructural features (see below). We note that these features augment the initial description of the Seidlwinkl Fold by Wolfgang Frank (1969). The fold was first geometrically modeled as a sheath fold by Hilty (2013) without any actual kinematic information to prove its origin as such. Along the lower limb of the Seidlwinkl fold nappe, the tectonostratigraphy is inverted, with the Rote Wand Nappe overlying the Glockner Nappe. The upper boundary of the sheath fold is taken to be the hanging wall of the D2 thrust between the Glockner Nappe s. str. (below)

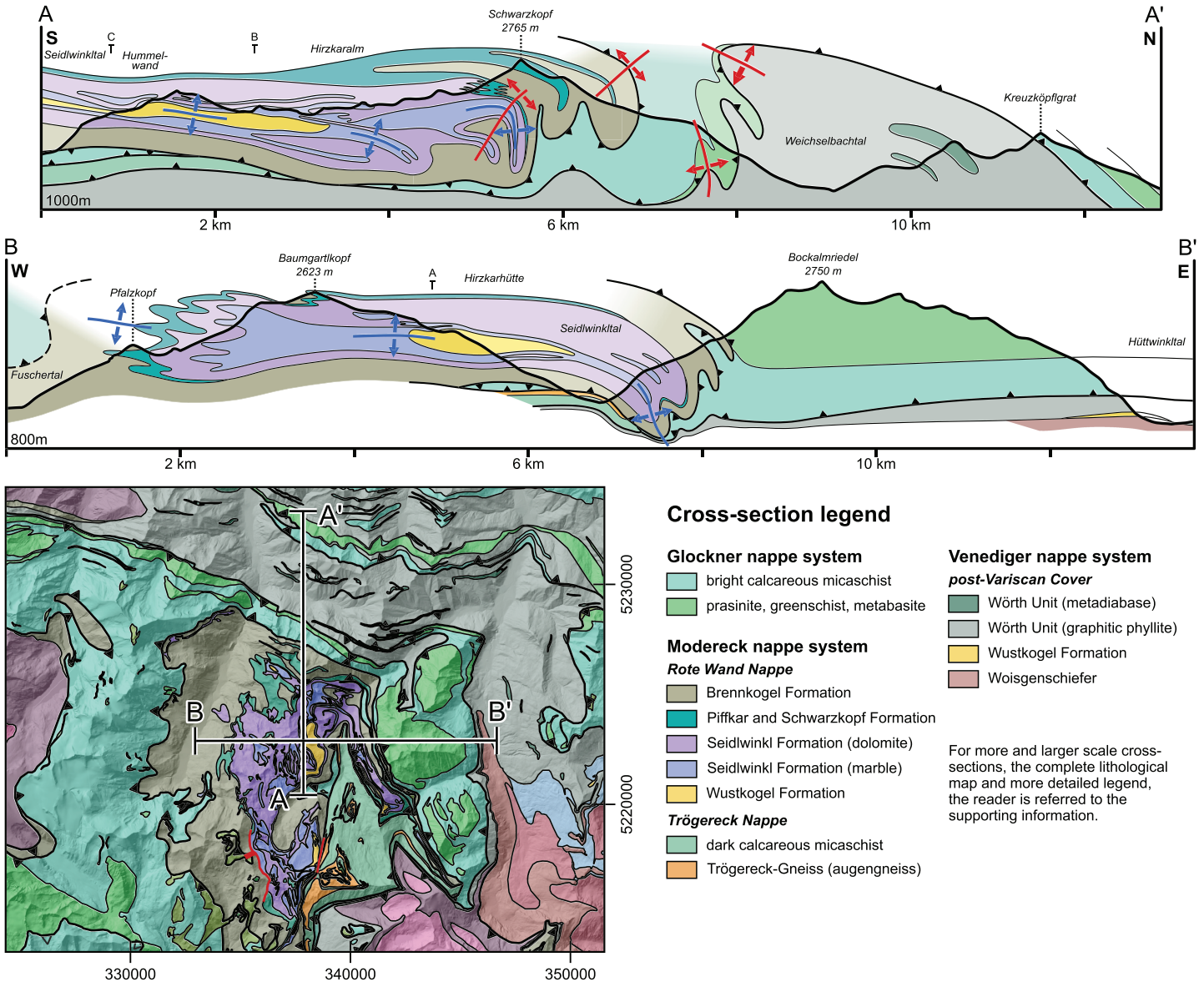

Figure 3. Exemplary cross sections through the nose of the isoclinal, recumbent Seidlwinkl sheath fold. Profile A-A' is parallel, and profile B-B' is perpendicular to the nappe transport direction. Note that the fold closes to the north, west, and east. More sections are found in the supporting information.

and the Rauris Nappe (above), because this thrust is not affected by D3 folding on the map scale. The Rauris Nappe does not occur in the lower limb of the Seidlwinkl sheath fold, and the Glockner Nappe is only exposed as far north as the steepened southern limb of the D4 Wörth antiform (Figure 4d and below). Thus, sheath folding affected only the Rote Wand Nappe and the Glockner Nappe s. str. but not the Rauris Nappe.

Axes of F3 parasitic isoclinal folds with amplitudes on the centimeter to meter scale generally trend N-S in most parts of the Seidlwinkl sheath fold. These minor folds deform lithological boundaries within the nappe as well as the D2 thrust between the Glockner Nappe and Rote Wand Nappe (e.g., Figure 3; Figure A2, profiles B–D) and include sheath folds (Figure 4b; Kurz et al., 1996). The opening angles of these F3 parasitic folds increase slightly from the core toward the perimeter of the Seidlwinkl fold nappe. In the limbs of these F3 folds, S2 and S3 form a composite S2-S3 foliation; S2 and S3 can only be distinguished in the hinges of F3 folds where S2 is tightly to isoclinally folded. A relict S2 is locally preserved as inclusions in garnet (Figure 4c); at garnet rims, this internal foliation is usually truncated by the S3 foliation in the matrix, as

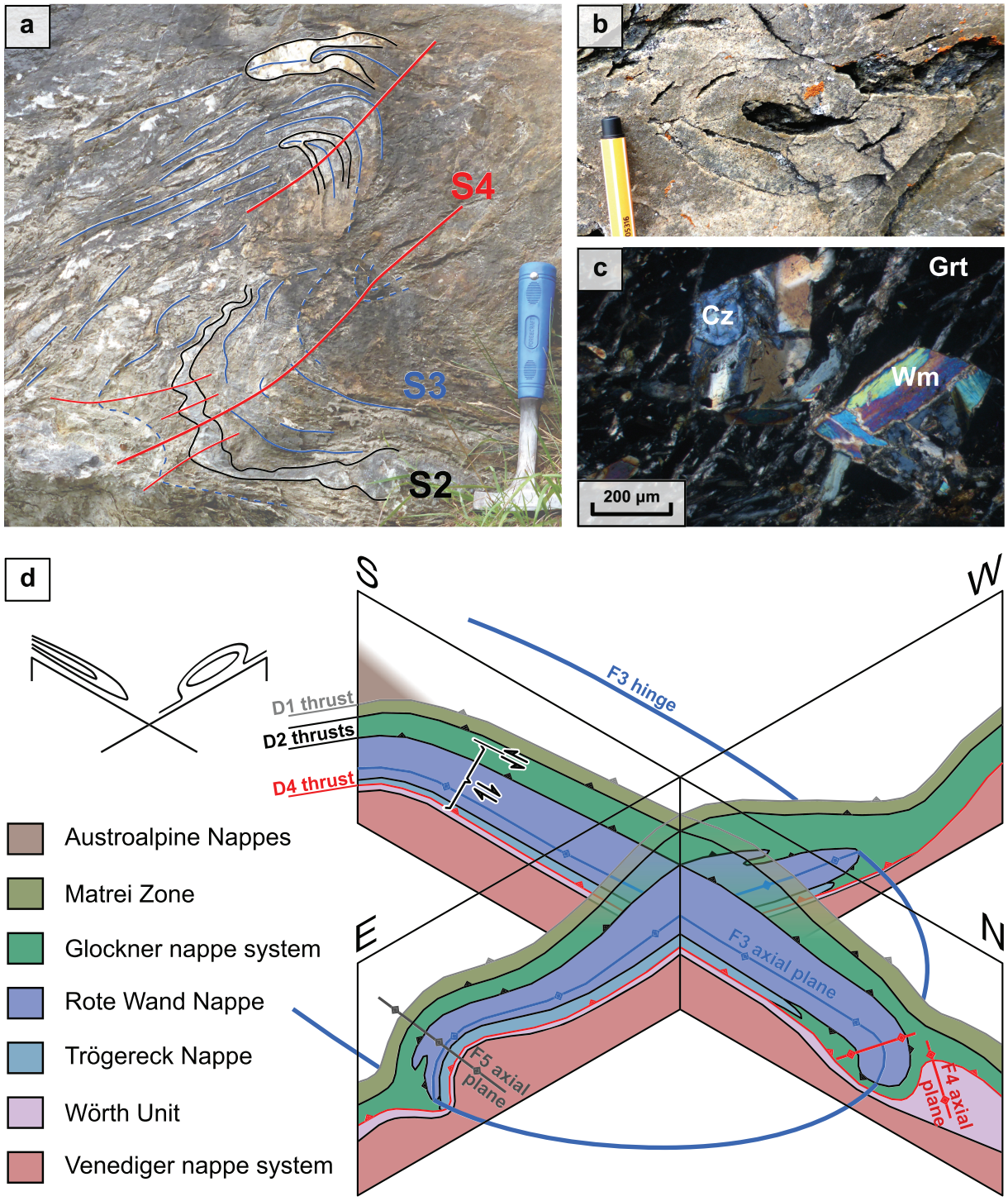

Figure 4. Structures of the Seidlwinkl sheath fold: (a) outcrop with cross-cutting relationships of D2, D3, and D4 structures; (b) sheath fold in quartzite with diagnostic eye-shaped pattern of concentrically folded layers in a section roughly perpendicular to the stretching lineation L3 marking the inferred transport direction; (c) microphotograph (crossed polarizers) of pseudomorphs of clinozoisite (Cz) and white mica (Wm) after lawsonite within garnet (Grt) from a garnet micaschist. Similar pseudomorphs also contain chlorite and albite (not shown here). The garnet also contains inclusions of chloritoid, rutile, and tourmaline; (d) block diagram of the Seidlwinkl sheath fold. Note that the D2 thrust is isoclinally folded by F3, which has a strongly curved hinge line. The fold has a concentric eye-shaped pattern and becomes omega-shaped toward its outer parts.

previously mentioned. Strain shadows near garnet porphyroblasts normally have a sigmoidal shape and consist of chlorite-quartz-phengite aggregates that are concordant with the S3 schistosity in the adjacent matrix (Figure 5). The microstructural observations above indicate that garnet growth initiated during late D2 and ceased before or during an early stage of D3.

A pronounced mineral stretching lineation, L3, is developed parallel to the F3 axes. L3 is defined by a shape-preferred orientation (SPO) of quartz, white mica, feldspar, calcite, or dolomite, depending on the lithology. L3 plunges variably, ranging from moderately S-plunging in the S, to flat-lying in the central part, to steeply N-plunging in the north.

Pervasive D3 shear sense indicators (e.g., shear bands, clasts, and crystallographic preferred orientation of quartz; Figures 6a and S4) yield top-N (i.e., top-to-the-foreland) motion in the entire Seidlwinkl sheath fold including the Glockner Nappe s.str, which is consistent with previous findings by Kurz et al. (1996). In the south of the study area, where the top of the fold is exposed (i.e., near the contact of the Glockner Nappe to the overlying Rauris Nappe), we observed sigma clasts (Figure 6b) and shear bands that locally overprint the pervasive top-N fabric. These have variable orientations but with predominant top-S (i.e., top-to-the-hinterland) sense of shear with a strong coaxial (flattening) component. In two localities (UTM 33N 330057 5214408 and 329117 5215107), we observed mutually overprinting ductile top-N and top-S shear bands, suggesting that both shear zones were at least partly contemporaneous, making the top-S shear zone a syn-D3 to post-D3 structure. Often, a brittle component of motion can be observed on the top-S shear bands, showing late reworking of the originally ductile fault or progressive cooling during continuous top-hinterland shearing. More examples of shear sense indicators on the outcrop-scale and microscale are found in Figures S3 and S4.

Primarily, in the nose of the Seidlwinkl sheath fold, D3 folds are deformed by E-W to SE-NW trending, open to tight F4 folds with a moderately N-dipping S4 axial plane cleavage (Figure 2a). This domain of steepened D3 structures occupies the southern limb of the D4 Wörth antiform (Figure 3, profile A; Figure A2, profile A), which was first recognized and named by W. Frank (personal communication). F4 fold axes plunge moderately to the W to NW. The Wörth antiform affects the parautochthonous cover of the Venediger basement and lies directly north of the steepened front of the Seidlwinkl fold nappe (Figure 3, profile A; Figure A2, profile A). In the hinge zone of the Wörth antiform and north thereof, the Venediger nappes are overthrusted by the Glockner nappe system. This thrust is interpreted as a late D3 to D4 thrust that emplaced the Rauris part of the Glockner nappe system onto the European margin represented by the Venediger nappe complex. The interference of D3 and D4 structures in this region causes meter-scale to kilometer-scale repetitions of lithologies and of the late D3 thrust between the Wörth Unit and the Glockner Nappe s. str.

The largest D5 structures in the study area, the Sonnblick Dome and Mallnitz Synform (Figure A1), deform the Seidlwinkl fold nappe and the main S2-S3 schistosity with its L3 stretching lineation (L3), so that the eastern part of the Seidlwinkl Fold is folded and stretched parallel to the NW-plunging L5 lineation (Favaro et al., 2017; Scharf, Handy, Favaro, et al., 2013; Figure 2e).

The age of deformation phases D2 to D5 is bracketed roughly by an $^{40}Ar/^{39}Ar$ phengite age from the Rote Wand Nappe that is interpreted to be the age of HP metamorphism at 39 Ma (Kurz et al., 2008) and by the onset of Adriatic indentation at ~21–23 Ma (Scharf, Handy, Favaro, et al., 2013).

4. Metamorphic Record in Metasediments

Microstructures allow us to determine the timing of mineral growth with respect to D3 deformation and formation of the Seidlwinkl sheath fold. In particular, the S3 schistosity is an excellent marker on which to apply pre-, syn-, and post-kinematic growth criteria in order to characterize the tectonometamorphic evolution and establish the physical conditions of nappe emplacement and folding. Pressure (P) and temperature (T) estimates were obtained by applying thermodynamic modeling of phase diagrams and Si-in-phengite isopleths as well as Raman spectroscopy on quartz inclusions (RSQI barometry; Ashley et al., 2014) and carbonaceous material (RSCM thermometry; calibration of Lünsdorf et al., 2017), methods that were shown to be suitable for our purpose (e.g., Bayet et al., 2018). We used a variety of lithologies including garnet micaschist (early Cretaceous Brennkogel Formation of the Rote Wand and Trögereck nappes and "Bündnerschiefer" of the Glockner Nappe) and chloritoid-bearing micaschist (late Triassic Piffkar Formation) of the Rote Wand

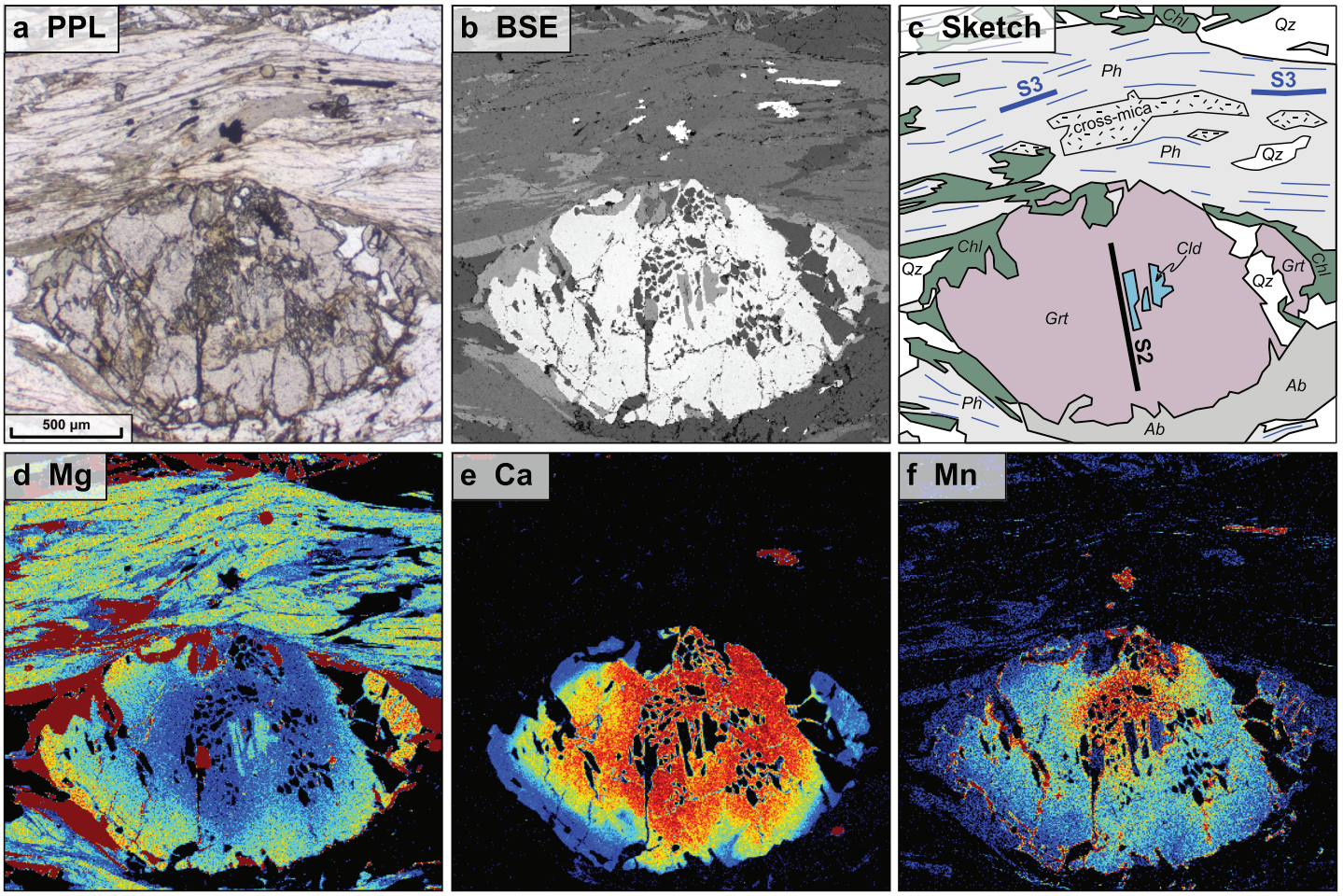

Figure 5. Microstructure of a garnet and adjacent areas in garnet micaschist of the Brennkogel Formation, sample PG89. (a) Transmitted light microphotograph with parallel polarizers; (b) backscatter electron image of the same grain; (c) sketch of the same area, showing the distribution of mineral phases and the two schistosities, S2 (Cld-SPO in Grt core) and S3 (main schistosity in matrix). Images (d) to (f) are element distribution maps for Mg, Ca, and Mn obtained with the electron microprobe, respectively. Color scale ranges from very low elemental abundance (black), intermediate abundance (light green), to very high abundance (dark red).

Nappe. The Mesozoic age of the protoliths guarantees that the *P-T* conditions pertain to the Alpine orogeny rather than Variscan and older events, while their microstructures record D3 kinematics. Readers are referred to the supporting information file for descriptions of the methods and procedures for obtaining *P-T* estimates from selected samples.

4.1. Microstructures and Parageneses

Garnet micaschists contain quartz, phengite, and chlorite, with albite, carbonate minerals, (clino-)-zoisite, epidote, paragonite, rutile, and titanite abundant but not ubiquitous, depending on bulk rock composition. Garnets often have inclusions of chloritoid and pseudomorphs after lawsonite (Figure 4c) that contain clinozoisite, paragonite, chlorite, and albite.

The garnets (Figure 5) commonly show prograde growth zoning, with Mn and Ca decreasing and Mg increasing from core to rim. Sometimes, a complex patchy enrichment in Ca can be observed in the outermost rims, which points toward late reequilibration or breakdown of Ca-bearing phases in the matrix (lawsonite?). The garnet grains are often strongly resorbed or replaced by newly grown chlorite.

In garnet micaschists, phengitic white mica is one of the main phases defining the main S2-S3 composite schistosity in the matrix but occasionally also occurs as cross micas oblique to this main foliation. The cores of grains from both phengite generations commonly are rich in Si with up to 3.47 Si p.f.u., whereas, along

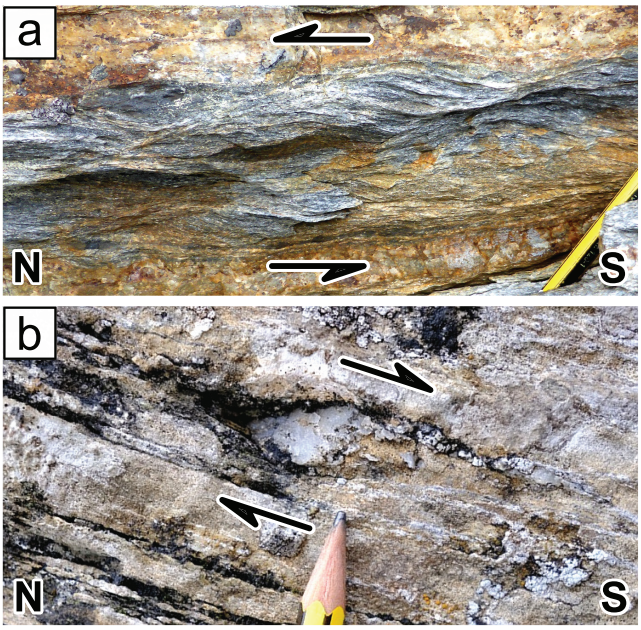

Figure 6. Shear sense indicators in the Seidlwinkl sheath fold. (a) Top-N shear bands to the main schistosity in micaschist (UTM 33N 342182 5208710). (b) Quartz sigma clast in marble indicating top-S sense of shear (UTM 33N 330380 5213630).

cleavage fractures and grain boundaries, the grains are locally replaced by mica with lower phengite content (down to ~3.05 Si p.f.u.). Consequently, each sample displays a broad range of mica compositions, from highly phengitic to almost purely muscovitic (Figure 7). This exchange is mainly controlled by Tschermak substitution; pyrophyllite substitution usually has a minor effect (K + Na always >0.85 p.f.u.).

The chloritoid micaschists contain quartz, phengitic white mica, chloritoid, ilmenite—occasionally with rutile in the core—and accessory allanite. These mineral phases usually have a strong shape-preferred orientation and thus define the main S2-S3 composite schistosity. Chlorite is relatively abundant, and kyanite-bearing varieties can be found as well; carbonate minerals and feldspar are lacking completely.

In chloritoid micaschists, white mica has a variable composition that ranges from phengite-rich mica (up to 3.33 Si p.f.u.) to muscovitic white mica. Samples that allow to discriminate S2-parallel mica from S3-parallel mica, for example, in F3 hinges where S2 and S3 are not parallel (Figure 7), revealed that micas from both generations show the same compositional variation between high and low phengite content. This may be caused by partial overprint of both mica generations, which also in this lithology is mainly controlled by Tschermak substitution; pyrophyllite substitution usually has a minor effect (K + Na always >0.85 p.f.u.). Chloritoid is relatively Fe rich, with Fe# (=Fe/(Fe + Mg + Mn)) ~0.80–0.95.

4.2. Constructing a *P-T-d* Path for the Seidlwinkl Nappe

Microstructural analysis combined with thermodynamic modeling, RSQI, and Si-in-phengite barometry allows us to derive a pressure-temperature-deformation (*P-T-d*) path for selected samples (detailed description in supporting information). In sample PG89 (Figure 8a), peak-*P* conditions of ~1.95 GPa at 520 °C are indicated by the peak assemblage chloritoid and high-Si phengite that grew shortly after the onset of garnet formation. Max-*P* quartz inclusions in garnet support this interpretation, yielding ~1.9 GPa as a pressure minimum during crystallization of garnet. At these conditions, the model predicts the stability of glaucophane and lawsonite, which were not found in the sample. However, the fact that the predicted modal abundance is very low (~1%) and that they may have been completely consumed by retrograde reactions may explain the slight discrepancy between model and observation. The peak-*P* event was associated with the development of the S2 schistosity defined as aligned chloritoid inclusions in garnet. The disappearance of chloritoid from the matrix, the beginning of garnet replacement by new chlorite, and the partial replacement of high-Si by low-Si phengite along grain boundaries and cleavage fractures (Figure 5) all indicate near-isothermal decompression to *P-T* conditions below the stability field of chloritoid at around 0.9 GPa and 500 °C. The paragenesis formed during early decompression defines the S3 main foliation. The maximum temperature is limited by the RSCM estimate to ~520 ± 30 °C. Retrograde metamorphism was accompanied by the development of the main S3 schistosity defined by the parallel alignment of phengite, chlorite, and quartz.

Sample PG61 shows a similar metamorphic evolution (Figure 8b). The thermodynamic model reproduces the observed peak-*P* mineral assemblage quartz, phengite, chloritoid, chlorite, garnet, and rutile in a well-defined stability field (1.5–1.85 GPa, 500–530 °C). The isopleths of measured maximum Si-in-phengite (max = 3.33 Si p.f.u.) intersect with the peak-assemblage stability field, further constraining peak-*P* conditions to at least ~1.6 GPa and 520 °C for equilibration of the high-Si phengite in the presence of chloritoid, chlorite, and garnet. Isothermal decompression to <1.5 GPa and <530 °C is documented by the incomplete replacement of high-Si by low-Si phengite, the breakdown of rutile to ilmenite (+geikielite), and the almost complete replacement of garnet by post-kinematic chloritoid.

Several aspects complicate straightforward thermodynamic modeling of complete *P-T* paths in most samples. These problematic aspects are, for example, fractionation of the bulk chemistry due to high garnet contents, pronounced kinetic effects leading to local disequilibria (e.g., metastable feldspar at HP conditions),

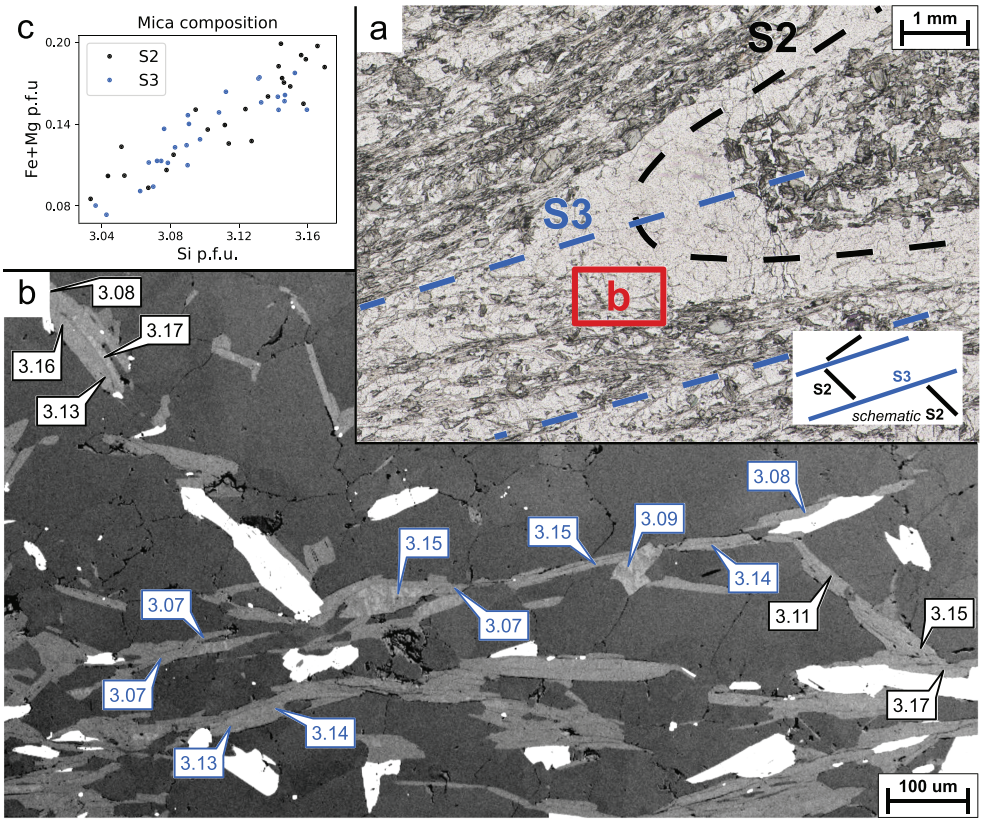

Figure 7. Compositional variation of white mica in sample PG130 (chloritoid-bearing micaschist of the Piffkar Formation, UTM Zone 33N: 335018 E, 5219912 N). (a) Thin section image of a fold hinge including sketch of the structural relationships; (b) backscatter electron (BSE) image of a part of the hinge region (red square in (a)), with Si (p.f.u.) content of phengite crystals from two microstructural generations S2 (black) and S3 (blue); (c) composition diagram for all mica analyses in this sample shows that both microstructural generations of white mica have the same range in phengite content.

high contents of ferric iron-rich minerals (epidote), and unclear effect of CO_2 activity in lithologies rich in organic carbon and carbonate minerals. Even though it may be possible to resolve these complications with sophisticated and elaborate thermodynamic modeling, we applied a simplified approach to efficiently get rough estimates for peak-*P* conditions. Given that constructed *P-T* paths (samples PG89 and PG61) show that (1) garnet formed close to peak-*P* conditions, (2) decompression was largely isothermal, and (3) no late thermal event exceeded the temperatures reached at peak *P*, we interpret the RSCM data to represent the *T* conditions close to peak *P*. Therefore, for most samples, we estimated the peak-*P* conditions by using the intersection of the RSCM temperature with either the RSQI pressure or Si-in-phengite isopleth. This procedure was performed on a suite of metasediment samples from the Glockner and Modereck nappe systems covering the whole study area. We consider the precision of peak-*P* values obtained by this procedure to be sufficient for our purpose of documenting the extent of HP metamorphism in the central Tauern Window.

4.3. *P-T* History of the Metasediments and Peak-*P* Map of the Central Tauern Window

In many investigated metasediment samples, an early low-*T* high-*P* (<500 °C, 1.3–2.0 GPa) phase is evidenced by relict pseudomorphs after lawsonite included in garnet (Figure 4c). Peak metamorphic conditions were reached in the garnet stability field. Minimum estimates for peak *P* are in the range of 1.3–2.3 GPa (Figure 9), which confirms the existence of an HP event for all samples investigated. For a majority of samples from both the Glockner and the Modereck nappe systems, the peak-*P* estimates converge to ~1.8–2.2 GPa. Somewhat lower peak *P* obtained for some of the samples, including PG61, may reflect incomplete preservation of the HP assemblages or Si loss of mica due to strong retrograde overprint or relaxation of quartz inclusions. The peak-*P* values of 1.8–2.2 GPa are somewhat higher than what is reported for metabasites

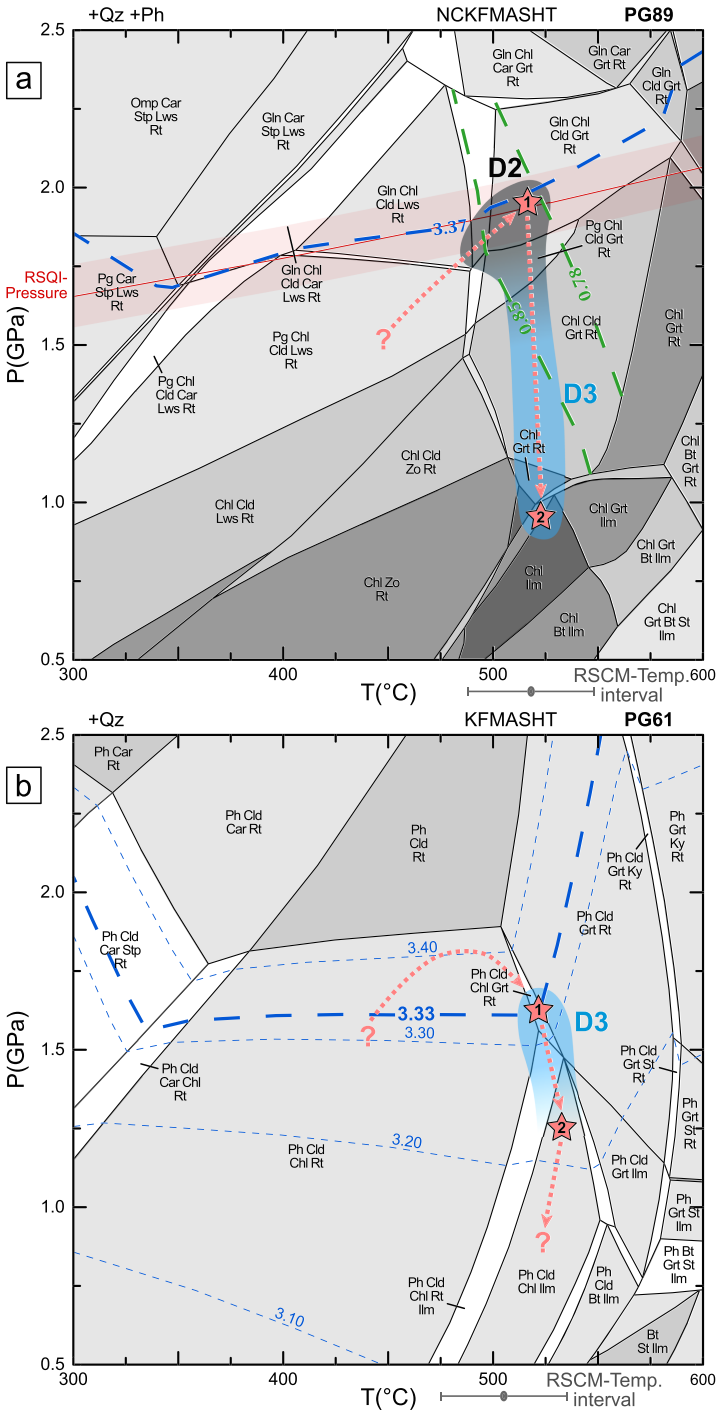

Figure 8. Pseudosections of sample PG89 (a) and PG61 (b) with inferred *P-T* path (dotted arrows). Dashed lines denote measured (thick) and calculated (thin) compositional isopleths for Si in phengite (blue, in a.p.f.u.) and XFe in chloritoid (green). Red solid line indicates the measured maximum pressure as a function of *T* as determined from RSQI, with the shaded red area indicating the uncertainty in the *P* estimate. Gray bracket denotes the measured RSCM temperature with its absolute uncertainty of ±30 °C. The black and/or blue shaded area shows the range of conditions during and after the D2 and D3 deformation. Red stars represent two distinct metamorphic stages. (a) PG89 stage 1: formation of peak-*P* mineral assemblage Grt, Cld, and high-Si phengite during regional D2 at ~520 °C and 1.95 GPa. Stage 2: near-isothermal decompression to <1.0 GPa (destabilization of Grt, Cld, and high-Si phengite). The model system composition is 80.51 SiO_2, 7.58 Al_2O_3, 5.00 FeO, 1.64 MgO, 0.28 CaO, 1.27 K_2O, 0.10 Na_2O, and 0.32 TiO_2 (all in wt%), with H_2O-saturated conditions. (b) PG61 stage 1: formation of peak-*P* mineral assemblage Qz, Ph, Cld, Chl, Grt, and Rt during D3 at ~520 °C and at least 1.6 GPa. Stage 2: near-isothermal decompression during and/or after D3 (decrease of Si content in matrix phengite, breakdown of matrix Rt to Ilm, and replacement of Grt by post-D3 Cld). The blue shaded area denotes the activity of the regional deformation phase D3 with respect to *P-T* conditions, as recorded in sample PG61. The model system composition is 67.43 SiO_2, 16.13 Al_2O_3, 8.70 FeO, 0.61 MgO, 1.51 K_2O, and 0.85 TiO_2 (all in wt%), with H_2O-saturated conditions.

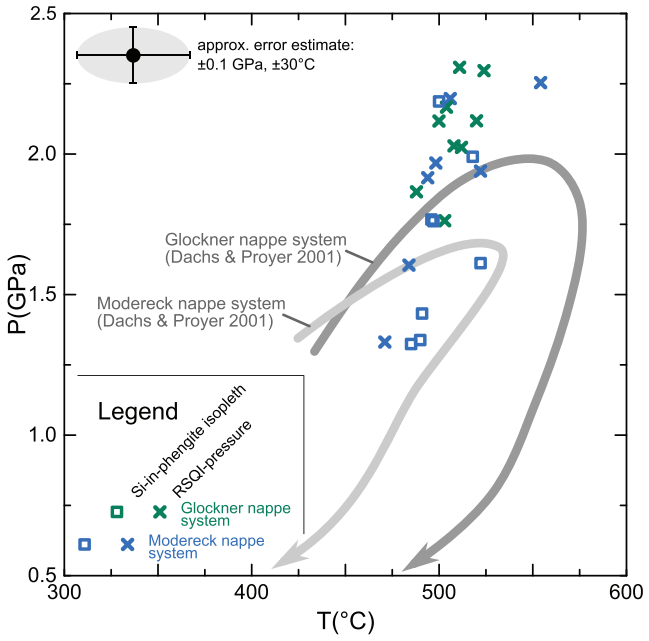

Figure 9. Peak-pressure metamorphic conditions obtained for metasediments from the Modereck and Glockner nappe systems using RSQI barometry and Si-in-phengite isopleths. RSQI values are minimum estimates.

from the Glockner Nappe (~1.8 GPa, Dachs & Proyer, 2001). The pressures derived from Si content of phengite tend to be somewhat lower than the RSQI pressures (Figure 9), and additionally, the S3 main foliation of some samples lacks diagnostic HP mineral phases that are still preserved as inclusions in garnet. Both observations reflect early stages of decompressional overprint of phengite and other matrix minerals during D3 top-foreland directed shear, which is not recorded by Qz inclusions in garnet. Later, stages of isothermal decompression to ~<1.0 GPa and 500 °C under low-strain conditions caused destabilization of garnet, transformation of rutile to ilmenite, and further partial overprint of phengite to almost pure muscovite.

In the map in Figure 10, we show the minimum estimates for peak-*P* conditions in metasediments. The continental Rote Wand and Trögereck nappes and the structurally lower part of the oceanic Glockner nappe system (Glockner Nappe s. str.) reached similar peak-*P* conditions of ~2.0 GPa. These conditions strongly contrast with those reached in the Venediger nappe system in the footwall where a much lower peak *P* of around 1 GPa at 530 °C is reported (Selverstone, 1993; Selverstone et al., 1984). The same applies to the Matrei Zone in the hanging wall where a peak *P* of 0.9–1.0 GPa at 360–370 °C has been inferred (Koller & Pestal, 2003) based on analogy of mineral assemblages and lithology with the Reckner Ophiolite (Dingeldey et al., 1997). However, the exact upper structural limit of eclogite-facies parageneses in the Glockner nappe system is ambiguous and has not been settled prior to this study. Following other authors (Frasl & Frank, 1964; Pestal & Hellerschmidt-Alber, 2011), we subscribe to the idea of a nappe boundary that separates the HP and low-pressure parts of the Glockner nappe system (i.e., between Glockner Nappe s. str. and Rauris Nappe, respectively). In the southern part of our study area, to the best of our knowledge, this nappe boundary has never been mapped before. We place it at the top of a thick prasinite layer that has a well-defined mid-ocean ridge basalt affinity (Höck & Miller, 1980) and is laterally largely continuous and can be found north and south of the central Tauern culmination. Structurally below this prasinite body, variegated parageneses contain HP metamorphic minerals with, for example, eclogite relicts in metabasites, lawsonite pseudomorphs in garnet, and two phengites in metasediments (own observations, Cornelius & Clar, 1934b; Frank et al., 1987). In the prasinite body itself lawsonite pseudomorphs were described (Frank et al., 1987); in addition, we found sparse remnants of strongly retrogressed eclogite. In the part of the Glockner nappe system structurally above the prasinite layer, no eclogite-facies parageneses have been found. This upper structural limit of eclogite-facies parageneses in the southern Tauern Window corresponds with the fabric boundary between pervasive top-N D3 shear fabrics below and top-S, syn- to post-D3 fabrics above.

5. Discussion

The results above indicate that the Seidlwinkl sheath fold nappe developed under retrograde conditions that involved a near-isothermal drop in pressure from a peak value of approximately 2.0 GPa to a residual pressure of roughly 1.0 GPa. Mylonitic shearing in this part of the Alpine subduction zone was pervasive, with the shear sense uniformly top-N (cf. Kurz et al., 1996), that is, transport direction of the upper, hanging wall limb toward the orogenic foreland. In the following, we address how the inherited geometry of the passive European margin caused sheath nappe folding during subduction and how this nappe fold was exhumed from within the subduction zone.

5.1. Formation of the Seidlwinkl Sheath Fold in the Alpine Subduction Zone

As shown in section 2 above, the Seidlwinkl Fold is very noncylindrical, with its axis curving almost 180° (Figures 2 and 3d). Yet its Triassic-to-lower Cretaceous cover derived from the former European passive margin survived subduction and collision remarkably intact. In most parts of the fold, this stratigraphic sequence

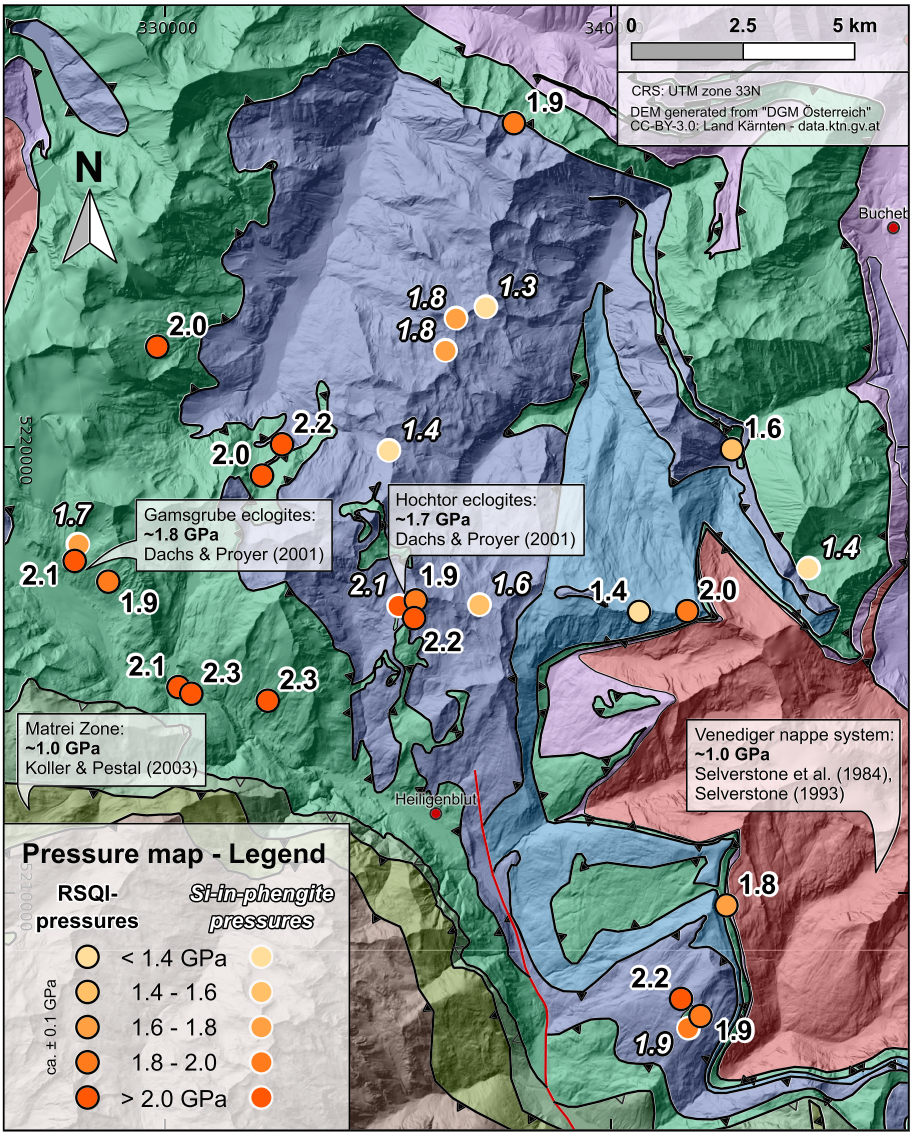

Figure 10. Distribution of peak-*P* estimates in metasediments of the central Tauern Window. RSQI values are minimum estimates. Tectonic units as in Figure 2.

is significantly thinned but only locally boudinaged, particularly the middle-Triassic dolomites. Mylonitic thinning and boudinage of the cover sequence are greater in the fold's lower limb.

The sheath fold does not exist along strike to the east and west in the Tauern Window, where only upward-younging passive-margin stratigraphy of the Modereck nappe system has been mapped around the perimeter of the Venediger nappe system (see, e.g., GK200 Salzburg, Pestal et al., 2005). Either the lower limb of the Seidlwinkl fold nappe was left behind to the south during top-N shearing and thrusting of the detached upper limb (i.e., a fold nappe in the sense of Heim, 1878, 1922), or a lower limb never existed in the eastern and western parts of the Tauern Window. So far, no relicts of an overturned limb have been found in the eastern and western Tauern Window, though we cannot rule out the possibility that such relics exist somewhere below the erosional surface.

This leaves us with the challenge of explaining why the sheath fold developed only in the central Tauern Window. Several mechanisms for the formation of sheath folds have been proposed so far: (a) amplification and/or rotation of a predeformational heterogeneity in the layer(s) during simple shearing (Cobbold & Quinquis, 1980). Possible heterogeneities include local variations in layer thickness or mechanical

properties or even a preexisting fold initially oriented oblique to the noncoaxial shearing plane; (b) perturbation of a highly noncoaxial flow field around strong inclusions (Marques & Cobbold, 1995; Rosas et al., 2002); or (c) perturbation near the tip of a planar, weak inclusion in a matrix of stronger, noncoaxially shearing rock (U. Exner & Dabrowski, 2010; Reber et al., 2012). All of these models involve overall simple shearing and fold amplification near a structural-rheological heterogeneity, but they do not explain how the heterogeneity forms to begin with. Moreover, noncylindrical nappes can develop where local strain rate varies perpendicular to the slip direction, as shown in studies of sheath folds formed during exhumation (Xypolias & Alsop, 2014) and as proposed for the Adula Nappe in the Central Alps (Kossak-Glowczewski et al., 2017). We cannot rule out the possibility that such gradients contributed to the formation of the Seidlwinkl sheath fold. However, any model for this fold must account for coeval top-foreland shearing in the main body of the fold and top-hinterland flow in its roof. We propose that sheath fold formation ultimately reflects lateral variations in thickness and composition of the rifted European margin. This in turn engendered along-strike differences in detachment level and fold style as the margin obliquely entered the Alpine subduction zone (Figure 11). The obliquity of subduction corresponds to the acute angle between the Paleogene NNW-SSE directed Adria-Europe convergence and the structural grain of the European passive margin, which formed during E-W rifting (Kurz et al., 1998) and opening of the northern part of Alpine Tethys (e.g., Frisch, 1979; Handy et al., 2010). In this scenario, the basement (Wustkogel gneiss) and cover of the Rote Wand Nappe in the core of the Seidlwinkl fold nappe originated as a rifted segment of the distal European continental margin (Figure 11a). This segment with relatively thick continental basement was separated from the main part of the European continental margin (future Venediger nappe system) by a rift basin with only thin basement (future Eclogite Zone and Trögereck Nappe). In this configuration, the rifted segment (future Rote Wand Nappe) formed a promontory of the margin that later acted as the nucleus for the Seidlwinkl sheath fold. As the passive margin approached the subduction zone, the ocean continent transition was likely a first-order mechanical heterogeneity due to the pronounced viscous strength contrast between thin continental units (mostly continental basement, siliciclastics, prerift platform carbonates, and postrift hemipelagic clastics of the Rote Wand Nappe) and oceanic lithosphere (serpentinized exhumed mantle and overlying mafics and hemipelagic sediments of the Glockner Nappe s. str.). Subduction of a promontory of the distal continental margin formed the composite ocean continent nappe stack, which then detached along the base of the Permian clastics (Wustkogel Formation) as the promontory entered the subduction zone (Figure 11b). Thrusting gave way to buckling and the formation of an embryonic Seidlwinkl Fold while the composite nappe stack was still at sufficiently low temperatures to favor high strength contrasts (>5) between the layers of the nappe stack (e.g., Evans & Kohlstedt, 1995; Ramberg, 1964). The fold became tighter with progressive noncoaxial shearing close to peak-pressure conditions at great depth in the subduction channel, where increasing temperature led to a drop in viscous strength contrast. Continued uniform, top-N shearing of all parts of the fold promoted passive amplification of the fold and accentuation of its noncylindrical sheath geometry (e.g., Dell'Ertole & Schellart, 2013; Marques et al., 2008) shortly after the attainment of peak-pressure conditions (Figure 11c). In essence, the formation of the Seidlwinkl sheath fold is the result of lateral variations in the structure of the European continental margin that provided an initial perturbation for nucleation of the fold. Modeling studies show that the width of such an initial perturbation controls the width of the subsequent sheath fold (Brun & Merle, 1988). This seems reasonable in light of our observations: The fold has an E-W width on the order of 20–30 km, which suggests that the width of the promontory—measured parallel to the later subduction zone—had a similar extent (Figure 11a). Several tens of kilometres is a common size for extensional allochthons or similar features ("H-blocks" of Péron-Pinvidic & Manatschal, 2010). However, we note that this model for the formation of the Seidlwinkl sheath fold is necessarily speculative in the absence of better preserved relicts. Recently, field-based studies have identified similar, highly noncylindrical nappes in the Alps (Kossak-Glowczewski et al., 2017; Steck et al., 2019).

5.2. Exhuming the Seidlwinkl Sheath Fold Nappe

Our new data show that imbricated and folded continental crust (Modereck nappe system) and oceanic crust (Glockner Nappe s. str.) experienced identical HP conditions of ~2 GPa during Alpine subduction, followed by the incorporation of these units in the Seidlwinkl sheath fold nappe during decompressional metamorphism. They were eventually emplaced to their current position in the nappe stack between other units that experienced lower peak pressures of ~1 GPa, that is, in the Matrei Zone and Rauris Nappe above and the

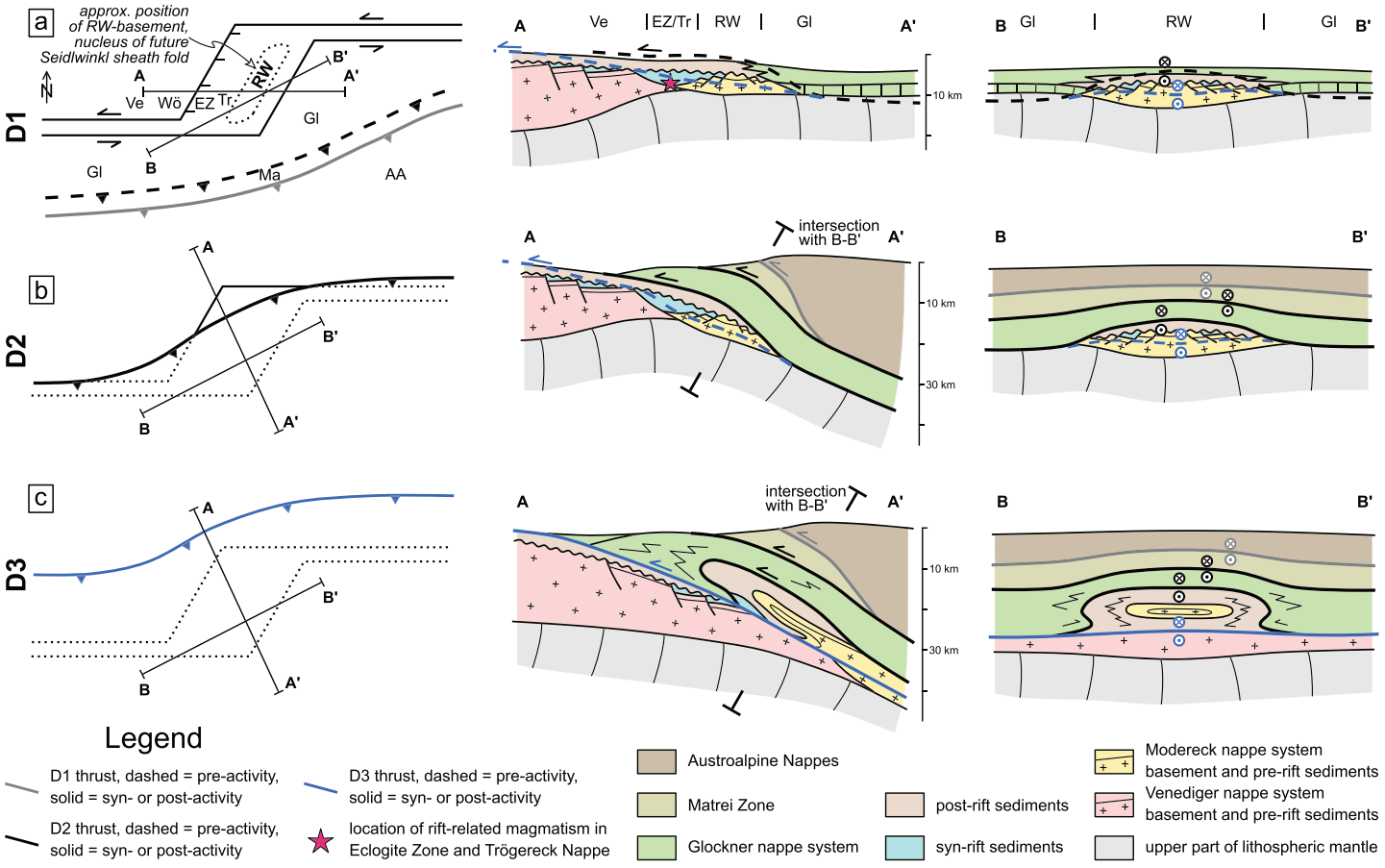

Figure 11. Formation of the Seidlwinkl sheath fold nappe. First column shows the evolving paleogeography in map view (inspired by Weissert & Bernoulli, 1985): (a) D1 convergence and oceanic subduction; (b) D2 prior to the baric peak; and (c) D3 after the baric peak in map view. Second and third columns are schematic cross sections of the margin corresponding to the traces on the maps. (a) Early subduction of Alpine Tethys. The future Rote Wand Nappe originated as a rifted segment of continental basement and cover and was separated from the main part of the margin by a rift basin (future Trögereck Nappe and Eclogite Zone); (b) beginning subduction of the distal European margin. The Rote Wand rift segment was thrust below the Glockner nappe system and further subducted; (c) Glockner and Rote Wand nappes become a composite sheath fold nappe fold in a noncoaxial shear zone. The width of the Rote Wand rift segment (=structural perturbation; sections B-B') dictates the width of the sheath fold. Abbreviations: Ve = Venediger nappe system (European margin), Wö = Wörth Unit, EZ = Eclogite Zone, Tr = Trögereck Nappe, RW = Rote Wand Nappe, Gl = Glockner nappe system, Ma = Matrei Zone, AA = Austroalpine nappes (Adriatic margin). Maps and sections are not drawn to scale; thickness of the units is exaggerated for clarity.

Venediger nappes below (Koller & Pestal, 2003; Selverstone, 1993; Selverstone et al., 1984). This 1-GPa difference in peak pressure is consistent with the observation that the HP Seidlwinkl Fold, which underwent pervasive top-N shearing, is bounded in its upper limb by a normal-sense shear zone that at least partly overprinted the lower-*P* Rauris Nappe. We propose that these shear zones—a thrust below and a normal fault above—were responsible for differential exhumation of the fold with its HP assemblages in the sense of a channel-extrusion model. This exhumation model requires that the two opposite-sense shear zones between which the rocks were exhumed were active simultaneously and that normal-sense shearing started at peak-pressure conditions. Contemporaneity of the opposite-sense shear zones is indicated at the top of the Seidlwinkl Fold by mutually overprinting top-N and top-S shear bands. We therefore interpret this top-S normal-sense shearing to have begun later than the initiation of D2 top-N shearing in the Glockner nappe system but to have been broadly coeval with D3 top-N thrusting in the Seidlwinkl Fold. We regard the parallelism of syn-decompressional, D3 top-N shearing planes in the entire Seidlwinkl Fold with the normal-sense, top-S shearing planes of the Rauris Nappe as a viable kinematic criterion for broadly contemporaneous activity of opposite-sense shearing during exhumation. This also means that the top-S shear zone was active during decompression but does not unequivocally prove that top-S shearing started at peak-pressure conditions, which, however, we consider plausible.

These kinematics raise the question of the forces driving exhumation of the HP Seidlwinkl Fold. Buoyancy forces have been suggested for the exhumation of HP nappes (e.g., Chemenda et al., 1995) in subduction channels. However, this is implausible in the case of the Seidlwinkl fold nappe because the density contrasts between the HP lithologies in this fold nappe (mostly carbonaceous Bündnerschiefer) and the lithologies of underlying and overlying units (marbles and granitoids) are negligible and may even favor negative buoyancy of the HP lithologies. Moreover, it has been argued that exhumation of HP rocks mainly by buoyancy requires large-scale extension of the upper plate driven by slab rollback (e.g., Brun & Faccenna, 2008), which may not have been the case during the final stages of subduction of Alpine Tethys and incipient exhumation of the Seidlwinkl sheath fold.

Another commonly invoked exhumation mechanism for HP rocks is channel extrusion, which involves their exhumation within a subduction channel with parallel or tapered walls. This extrusion is forced by convergence of the walls and/or noncoaxial shearing parallel to the walls (e.g., Escher & Beaumont, 1997; Grujic et al., 1996; Grujic & Mancktelow, 1995; Mancktelow, 1995, 2008; Vannay & Grasemann, 2001). In such models, flow in the channel is driven by a pressure gradient parallel to the channel that is related to the variable rates of convergence and shearing, respectively, across and along the channel. The walls of the channel are assumed to be strong compared to the channel. The models usually show exhumation of HP rocks between coeval shear zones with opposite shearing senses, similar to those observed in the Seidlwinkl fold nappe and its roof. Thus, the channel-extrusion model elegantly explains how the Seidlwinkl Fold formed during top-foreland shearing while being exhumed in the footwall of a top-hinterland shear zone.

A consequence of the channel flow model is that the pressure gradient along the channel required to sustain upward flow of the extruding rock inevitably causes a dynamic pressure component in addition to the lithostatic pressure. The combined lithostatic and dynamic pressure in the channel is higher than in the stronger walls. The magnitude of this dynamic pressure component depends on the geometry of the channel (length, thickness, and angle between the confining walls), the strain rate, the channel viscosity, and the viscosity contrast between weak channel and walls (Mancktelow, 1995, 2008). The tectonically induced pressure gradient must be sustained for the duration of exhumation; otherwise, the upward flow of the exhuming material ceases. Mancktelow (2008) calculated dynamic pressures on the order of several hundred MPa for a tapered channel geometry, assumed natural shear displacement rate and viscosity contrasts.

Applying models like this to the Seidlwinkl fold nappe is speculative endeavor because only the top part of the subduction channel is exposed at the surface today; the original channel geometry cannot be restored. This precludes using the approach above to calculate the dynamic pressure and its contribution to pressure recorded by mineral parageneses in the Seidlwinkl sheath fold. The units overlying and underlying the HP-bearing Seidlwinkl fold nappe comprise weak carbonates and calc-schists that could not have acted as strong confining channel walls, suggesting that the component of dynamic pressure was small. However, at greater depth within the channel, the dynamic pressure may have been higher if the adjacent wall rocks (basement?) are assumed to have been more viscous. A parameter study exploring the potential range of conditions at depth is beyond the scope of this study.

Dynamic pressure variations can also be expected near rheological heterogeneities that cause variations in the differential stress. In the case investigated here, pronounced lithological and rheological heterogeneities are not apt to cause pronounced changes in recorded pressures. For example, peak pressures in weak metasediments are very similar to those reported for stronger metabasite lenses and layers (Dachs & Proyer, 2001). If this observation is not caused by sampling bias, it indicates that dynamically induced variations in peak P within the Seidlwinkl sheath fold nappe are probably smaller than the uncertainties of the available pressure estimates.

6. Conclusion

We have documented a recumbent, crustal-scale sheath fold in the central Tauern Window. The fold itself is a composite structure, comprising an isoclinally folded thrust of the former Alpine Tethys (Glockner Nappe s. str.) onto the former European continental margin (Rote Wand Nappe). The pervasive foliation in the area is parallel to the axial plane of the fold and carries an N-S oriented stretching lineation with top-N (to foreland) shear indicators. New petrological data show that both the oceanic and continental nappes experienced identical peak-pressure conditions of roughly 2.0 GPa and 500 °C, followed by isothermal

decompression during top-N shearing. These conditions are remarkably higher than the peak-*P* conditions reported for the tectonic units in the footwall and hanging wall of the sheath fold.

The kinematic observations are compatible with the classical theory of sheath fold formation by passive amplification of a preexisting perturbation under high-strain simple shear deformation (Cobbold & Quinquis, 1980). Based on regional lithostratigraphic correlation, we propose that this initial perturbation was inherited from lateral variations in the structure and stratigraphy of the rifted European margin. A rifted segment of the passive margin—similar to an extensional allochthon as suggested by Kurz (2006)—composed of Rote Wand Nappe basement and cover formed a structural promontory that was passively amplified to a sheath fold geometry with progressive top-foreland directed shearing in the Alpine subduction zone.

The Seidlwinkl sheath fold nappe is bounded at its top by a top-hinterland (top-S) shear zone with a strong component of flattening. This top-hinterland shear zone also generally coincides with the boundary between the eclogite-bearing (Glockner s. str.) and eclogite-free (Rauris) units. The fold itself exhibits intense and pervasive top-foreland (top-N) kinematics. These opposite-sense shear zones accommodated differential exhumation of the HP sheath fold nappe relative to the surrounding low-pressure tectonic units (Rauris Nappe above, Venediger nappe system below) in the sense of channel-extrusion exhumation models, where the weak, exhuming rock body is separated from the units above and below by a normal fault and a thrust, respectively. At greater depths in the subduction channel not accessible to observation, we infer that the exhuming sheath fold nappe may have been surrounded by stronger wall rocks and therefore have experienced a nonlithostatic pressure gradient driving its exhumation (Mancktelow, 2008).

This study highlights how features inherited from passive margins may dictate the geometry of nappes formed during accretion and subduction of continental margins. In comparable settings, the lateral variability of margins will strongly affect the internal configuration of subduction zones and collisional orogens like the Alps or Himalayas. Orogen-scale two-dimensional cross sections or seismological profiles do not fully account for such lateral heterogeneity and might therefore misleadingly imply a higher degree of cylindricity than in nature.

Acknowledgments
We thank Anja Schleicher and Andrea Gottsche (both GFZ Potsdam) for providing XRF measurements and Anna Giribaldi for excellent sample preparation. We thank the Geological Survey of Austria (Geologische Bundesanstalt—GBA) for providing access to unpublished maps and greatly acknowledge helpful discussions with our colleagues from the GBA Wolfgang Frank, Benjamin Huet, Ralf Schuster, and Christoph Iglseder. The manuscript benefitted substantially from constructive reviews by an anonymous reviewer and Neil Mancktelow. We thank editor Margaret Rusmore and associate editor Lothar Ratschbacher for swift editorial handling. This research was funded by the Deutsche Forschungsgemeinschaft (DFG) as part of the priority program SPP 2017 "Mountain Building in Four Dimensions (MB-4D)" (Grants PL 534/4-1, JO 349/11-1, and HA 2403/24-1) and part of the AlpArray Working Group. The supporting information contains additional details on the methods used, high-resolution versions of maps and cross sections, and data tables. The data tables are stored in the GFZ Data Services repository (Groß et al., 2020; http://doi.org/10.5880/fidgeo.2020.010).

References

Agard, P., Plunder, A., Angiboust, S., Bonnet, G., & Ruh, J. (2018). The subduction plate interface: Rock record and mechanical coupling (from long to short timescales). *Lithos*, *320*, 537–566.

Agard, P., Yamato, P., Jolivet, L., & Burov, E. (2009). Exhumation of oceanic blueschists and eclogites in subduction zones: Timing and mechanisms. *Earth-Science Reviews*, *92*(1-2), 53–79.

Alber, J. (1974). Seriengliederung, metamorphose und tektonik des Hocharngebietes (Rauristertal/Salzburg). Universität Wien.

Ashley, K. T., Caddick, M. J., Steele-MacInnis, M. J., Bodnar, R. J., & Dragovic, B. (2014). Geothermobarometric history of subduction recorded by quartz inclusions in garnet. *Geochemistry, Geophysics, Geosystems*, *15*, 350–360. https://doi.org/10.1002/2013GC005106

Babist, J., Handy, M. R., Konrad-Schmolke, M., & Hammerschmidt, K. (2006). Precollisional, multistage exhumation of subducted continental crust: The Sesia Zone, Western Alps. *Tectonics*, *25*, TC6008. https://doi.org/10.1029/2005TC001927

Bauville, A., & Schmalholz, S. M. (2015). Transition from thin- to thick-skinned tectonics and consequences for nappe formation: Numerical simulations and applications to the Helvetic nappe system, Switzerland. *Tectonophysics*, *665*, 101–117.

Bayet, L., John, T., Agard, P., Gao, J., & Li, J.-L. (2018). Massive sediment accretion at 80 km depth along the subduction interface: Evidence from the southern Chinese Tianshan. *Geology*, *46*(6), 495–498.

Beaumont, C., Fullsack, P., & Hamilton, J. (1994). Styles of crustal deformation in compressional orogens caused by subduction of the underlying lithosphere. *Tectonophysics*, *232*(1), 119–132.

Beltrando, M., Rubatto, D., & Manatschal, G. (2010). From passive margins to orogens: The link between ocean-continent transition zones and (ultra) high-pressure metamorphism. *Geology*, *38*(6), 559–562.

Bousquet, R., Goffé, B., Henry, P., Le Pichon, X., & Chopin, C. (1997). Kinematic, thermal and petrological model of the Central Alps: Lepontine metamorphism in the upper crust and eclogitisation of the lower crust. *Tectonophysics*, *273*(1-2), 105–127.

Bousquet, R., Oberhansli, R., Schmid, S., Berger, A., Wiederkeher, M., Robert, C., et al. (2012). Metamorphic framework of the Alps-Carte metamorphique des Alpes CCGM/CGMW: CCGM/CGMW.

Brun, J.-P., & Faccenna, C. (2008). Exhumation of high-pressure rocks driven by slab rollback. *Earth and Planetary Science Letters*, *272*(1), 1–7. https://doi.org/10.1016/j.epsl.2008.02.038

Brun, J.-P., & Merle, O. (1988). Experiments on folding in spreading-gliding nappes. *Tectonophysics*, *145*(1-2), 129–139.

Burov, E., Jolivet, L., Le Pourhiet, L., & Poliakov, A. (2001). A thermomechanical model of exhumation of high pressure (HP) and ultra-high pressure (UHP) metamorphic rocks in Alpine-type collision belts. *Tectonophysics*, *342*(1-2), 113–136.

Chapple, W. M. (1978). Mechanics of thin-skinned fold-and-thrust belts. *Geological Society of America Bulletin*, *89*(8), 1189–1198.

Chemenda, A. I., Mattauer, M., Malavieille, J., & Bokun, A. N. (1995). A mechanism for syn-collisional rock exhumation and associated normal faulting: Results from physical modelling. *Earth and Planetary Science Letters*, *132*(1), 225–232.

Chopin, C. (1984). Coesite and pure pyrope in high-grade blueschists of the Western Alps: A first record and some consequences. *Contributions to Mineralogy and Petrology*, *86*(2), 107–118.

Cliff, R. A., Droop, G. T. R., & Rex, D. C. (1985). Alpine metamorphism in the south-east Tauern Window, Austria: 2. Rates of heating, cooling and uplift. *Journal of Metamorphic Geology*, *3*(4), 403–415.

Cobbold, P. R., & Quinquis, H. (1980). Development of sheath folds in shear regimes. *Journal of Structural Geology*, *2*(1), 119–126.
Cornelius, H. P., & Clar, E. (1934a). *Erläuterungen zur geologischen Karte des Großglocknergebietes*. Wien: Geologische Bundesanstalt.
Cornelius, H. P., & Clar, E. (1934b). *Geologische Karte des Großglocknergebietes*. Wien: Geologische Bundesanstalt.
Dachs, E., Kurz, W., & Proyer, A. (2005). Alpine eclogites in the Tauern Window. *Mitteilungen der Österreichischen Mineralogischen Gesellschaft*, *150*, 199–226.
Dachs, E., & Proyer, A. (2001). Relics of high-pressure metamorphism from the Grossglockner region, Hohe Tauern, Austria. *European Journal of Mineralogy*, *13*(1), 67–86.
Dahlen, F. A., Suppe, J., & Davis, D. (1984). Mechanics of fold-and-thrust belts and accretionary wedges: Cohesive Coulomb theory. *Journal of Geophysical Research*, *89*(B12), 10,087–10,101.
Davies, J. H., & von Blanckenburg, F. (1995). Slab breakoff: A model of lithosphere detachment and its test in the magmatism and deformation of collisional orogens. *Earth and Planetary Science Letters*, *129*(1-4), 85–102.
Dell'Ertole, D., & Schellart, W. P. (2013). The development of sheath folds in viscously stratified materials in simple shear conditions: An analogue approach. *Journal of Structural Geology*, *56*, 129–141.
Dingeldey, C., Dallmeyer, R. D., Koller, F., & Massonne, H.-J. (1997). P-T-t history of the Lower Austroalpine Nappe Complex in the "Tarntaler Berge" NW of the Tauern Window: Implications for the geotectonic evolution of the central Eastern Alps. *Contributions to Mineralogy and Petrology*, *129*(1), 1–19.
Droop, G. T. R. (1985). Alpine metamorphism in the south-east Tauern Window, Austria: 1. P-T variations in space and time. *Journal of Metamorphic Geology*, *3*(4), 371–402.
Escher, A., & Beaumont, C. (1997). Formation, burial and exhumation of basement nappes at crustal scale: A geometric model based on the Western Swiss-Italian Alps. *Journal of Structural Geology*, *19*(7), 955–974.
Evans, B., & Kohlstedt, D. L. (1995). Rheology of rocks. Rock Physics and Phase Relations: A Handbook of Physical Constants, AGU Ref. Shelf, 3, 148–165.
Exner, C. (1957). *Erläuterungen zur geologischen Karte der Umgebung von Gastein*. Wien: Geologische Bundesanstalt.
Exner, C. (1964). *Erläuterungen zur geologischen Karte der Sonnblickgruppe 1:50000*. Wien: Geologische Bundesanstalt.
Exner, U., & Dabrowski, M. (2010). Monoclinic and triclinic 3D flanking structures around elliptical cracks. *Journal of Structural Geology*, *32*(12), 2009–2021. https://doi.org/10.1016/j.jsg.2010.08.002
Favaro, S., Handy, M. R., Scharf, A., & Schuster, R. (2017). Changing patterns of exhumation and denudation in front of an advancing crustal indenter, Tauern Window (Eastern Alps). *Tectonics*, *36*, 1053–1071. https://doi.org/10.1002/2016TC004448
Favaro, S., Schuster, R., Handy, M. R., Scharf, A., & Pestal, G. (2015). Transition from orogen-perpendicular to orogen-parallel exhumation and cooling during crustal indentation—Key constraints from $^{147}Sm/^{144}Nd$ and $^{87}Rb/^{87}Sr$ geochronology (Tauern Window, Alps). *Tectonophysics*, *665*, 1–16.
Frank, W. (1965). Zur Geologie des Guggernbachtales. Dissertation Univ Wien.
Frank, W. (1969). Geologie der Glocknergruppe. *Wissenschaftliche Alpenvereinshefte des Deutschen Alpenvereins*, *21*, 95–111.
Frank, W., Höck, V., & Miller, C. (1987). Metamorphic and tectonic history of the central Tauern Window. Geodynamics of the Eastern Alps, 34–54.
Frasl, G., & Frank, W. (1964). Exkursion I/2: Mittlere Hohe Tauern. *Mitteilungen der Geologischen Gesellschaft in Wien*, *57*(1), 17–31.
Frasl, G., & Frank, W. (1966). Einführung in die Geologie des Penninikums im Tauernfenster mit besonderer Berücksichtigung des Mittelabschnittes im Oberpinzgau. Der Aufschluß, Sonderheft, 15.
Frisch, W. (1979). Tectonic progradation and plate tectonic evolution of the Alps. *Tectonophysics*, *60*(3-4), 121–139.
Frisch, W., Gommeringer, K., Kelm, U., & Popp, F. (1987). The Upper Bündner Schiefer of the Tauern Window—A key to understanding Eoalpine orogenic processes in the Eastern Alps. *Geodynamics of the Eastern Alps*, 55–69.
Froitzheim, N., & Manatschal, G. (1996). Kinematics of Jurassic rifting, mantle exhumation, and passive-margin formation in the Austroalpine and Penninic nappes (eastern Switzerland). *Geological Society of America Bulletin*, *108*(9), 1120–1133.
Gebauer, D. (1999). Alpine geochronology of the Central and Western Alps: New constraints for a complex geodynamic evolution. *Schweizerische Mineralogische und Petrographische Mitteilungen*, *79*(1), 191–208.
Gerya, T. (2015). Tectonic overpressure and underpressure in lithospheric tectonics and metamorphism. *Journal of Metamorphic Geology*, *33*(8), 785–800.
Groß, P., Handy, M., John, T., Pestal, G., & Pleuger, J.. (2020). Mineral chemistry of metapelites from the Modereck Nappe (central Tauern Window, Eastern Alps): GFZ Data Services. Retrieved from http://doi.org/10.5880/fidgeo.2020.010
Grujic, D., Casey, M., Davidson, C., Hollister, L. S., Kündig, R., Pavlis, T., & Schmid, S. (1996). Ductile extrusion of the higher Himalayan crystalline in Bhutan: Evidence from quartz microfabrics. *Tectonophysics*, *260*(1), 21–43.
Grujic, D., & Mancktelow, N. S. (1995). Folds with axes parallel to the extension direction: An experimental study. *Journal of Structural Geology*, *17*(2), 279–291. https://doi.org/10.1016/0191-8141(94)E0048-4
Hacker, B. R., Gerya, T. V., & Gilotti, J. A. (2013). Formation and exhumation of ultrahigh-pressure terranes. *Elements*, *9*(4), 289–293.
Handy, M. R., Schmid, S. M., Bousquet, R., Kissling, E., & Bernoulli, D. (2010). Reconciling plate-tectonic reconstructions of Alpine Tethys with the geological-geophysical record of spreading and subduction in the Alps. *Earth-Science Reviews*, *102*(3), 121–158.
Handy, M. R., Ustaszewski, K., & Kissling, E. (2015). Reconstructing the Alps-Carpathians-Dinarides as a key to understanding switches in subduction polarity, slab gaps and surface motion. *International Journal of Earth Sciences*, *104*(1), 1–26.
Heim, A. (1878). Untersuchungen über den Mechanismus der Gebirgsbildung im Anschluss an die geologische Monographie der Tödi-Windgällen-Gruppe: Mit einem Atlas (Vol. 1): Schwabe.
Heim, A. (1922). Geologie der Schweiz (Vol. 2): CH Tauchnitz.
Hilty, L. (2013). 3D modeling of the Seidlwinkl-Nappe in the central Tauern Window, Austria (Bachelor Thesis). Universität Wien.
Höck, V., & Miller, C. (1980). Chemistry of mesozoic metabasites in the middle and eastern part of the Hohe Tauern. *Mitteilungen der Österreichischen Geologischen Gesellschaft*, *71*(72), 81–80.
Höck, V., & Pestal, G. (1994). GK50 Blatt 153 Grossglockner. Geologische Karte der Republik Österreich. Wien: Geologische Bundesanstalt.
Hoernes, S., & Friedrichsen, H. (1974). Oxygen isotope studies on metamorphic rocks of the Western Hohe Tauern area (Austria). *Schweizerische Mineralogische und Petrographische Mitteilungen*, *54*, 769–788.
Hoinkes, G., Koller, F., Rantitsch, G., Dachs, E., Hock, V., Neubauer, F., & Schuster, R. (1999). Alpine metamorphism of the Eastern Alps. *Schweizerische Mineralogische und Petrographische Mitteilungen*, *79*(1), 155–181.
Houseman, G. A., McKenzie, D. P., & Molnar, P. (1981). Convective instability of a thickened boundary layer and its relevance for the thermal evolution of continental convergent belts. *Journal of Geophysical Research*, *86*(B7), 6115–6132.

Jolivet, L., Faccenna, C., Goffé, B., Burov, E., & Agard, P. (2003). Subduction tectonics and exhumation of high-pressure metamorphic rocks in the Mediterranean orogens. *American Journal of Science*, *303*(5), 353–409.

Koller, F., & Pestal, G. (2003). Die ligurischen Ophiolite der Tarntaler Berge und der Matreier Schuppenzone. *Geologische Bundesanstalt—Arbeitstagung 2003: Blatt 148 Brenner*, 65–76.

Kossak-Glowczewski, J., Froitzheim, N., Nagel, T., Pleuger, J., Keppler, R., Leiss, B., & Régent, V. (2017). Along-strike shear-sense reversal in the Vals-Scaradra Shear Zone at the front of the Adula Nappe (Central Alps, Switzerland). *Swiss Journal of Geosciences*, *110*(2), 677–697.

Kurz, W. (2006). Penninic paleogeography from the Western toward the Eastern Alps—Still open questions? *International Geology Review*, *48*(11), 996–1022.

Kurz, W., Handler, R., & Bertoldi, C. (2008). Tracing the exhumation of the Eclogite Zone (Tauern Window, Eastern Alps) by $^{40}Ar/^{39}Ar$ dating of white mica in eclogites. *Swiss Journal of Geosciences*, *101*(1), 191–206.

Kurz, W., Neubauer, F., & Genser, J. (1996). Kinematics of Penninic nappes (Glockner Nappe and basement-cover nappes) in the Tauern Window (Eastern Alps, Austria) during subduction and Penninic-Austroalpine collision. *Eclogae Geologicae Helvetiae*, *89*(1), 573–605.

Kurz, W., Neubauer, F., Genser, J., & Dachs, E. (1998). Alpine geodynamic evolution of passive and active continental margin sequences in the Tauern Window (Eastern Alps, Austria, Italy): A review. *Geologische Rundschau*, *87*(2), 225–242.

Lammerer, B. (1986). Das Autochthon im Westlichen Tauernfenster. *Jahrbuch der Geologischen Bundesanstalt*, *129*(1), 51–67.

Lünsdorf, N. K., Dunkl, I., Schmidt, B. C., Rantitsch, G., & Eynatten, H. von (2017). Towards a higher comparability of geothermometric data obtained by Raman spectroscopy of carbonaceous material. Part 2: A revised geothermometer. Geostandards and Geoanalytical Research.

Mancktelow, N. S. (1993). Tectonic overpressure in competent mafic layers and the development of isolated eclogites. *Journal of Metamorphic Geology*, *11*(6), 801–812.

Mancktelow, N. S. (1995). Nonlithostatic pressure during sediment subduction and the development and exhumation of high pressure metamorphic rocks. *Journal of Geophysical Research*, *100*(B1), 571–583.

Mancktelow, N. S. (2008). Tectonic pressure: Theoretical concepts and modelled examples. *Lithos*, *103*(1), 149–177.

Marques, F. O., & Cobbold, P. R. (1995). Development of highly non-cylindrical folds around rigid ellipsoidal inclusions in bulk simple shear regimes: Natural examples and experimental modelling. *Journal of Structural Geology*, *17*(4), 589–602.

Marques, F. O., Guerreiro, S. M., & Fernandes, A. R. (2008). Sheath fold development with viscosity contrast: Analogue experiments in bulk simple shear. *Journal of Structural Geology*, *30*(11), 1348–1353.

Moulas, E., Podladchikov, Y. Y., Aranovich, L. Y., & Kostopoulos, D. (2013). The problem of depth in geology: When pressure does not translate into depth. *Petrology*, *21*(6), 527–538.

Oberhänsli, R., Bousquet, R., Engi, M., Goffé, B., Gosso, G., et al (2004). Metamorphic structure of the Alps. *CCGM (Commission of the Geological Maps of the World),* Paris.

Okay, A. I., Xu, S., & Sengor, A. C. (1989). Coesite from the Dabie Shan eclogites, central China. *European Journal of Mineralogy*, *1*(4), 595–598.

Péron-Pinvidic, G., & Manatschal, G. (2010). From microcontinents to extensional allochthons: Witnesses of how continents rift and break apart? *Petroleum Geoscience*, *16*(3), 189–197.

Pestal, G. (2008). Bericht 2006 und 2007 über geologische Aufnahmen auf Blatt 154 Rauris. *Jahrbuch der Geologischen Bundesanstalt*, *148*(2), 262–264.

Pestal, G., Hejl, E., Egger, H., van Husen, D., Linner, M., Mandl, M., et al. (2005). *Geologische Karte von Salzburg 1:200000*. Wien: Geologische Bundesanstalt.

Pestal, G., & Hellerschmidt-Alber, J. (2011). Bericht 2009 und 2010 über geologische Aufnahmen auf Blatt 154 Rauris. *Jahrbuch der Geologischen Bundesanstalt*, *151*(1 + 2), 142–147.

Petrini, K., & Podladchikov, Y. (2000). Lithospheric pressure-depth relationship in compressive regions of thickened crust. *Journal of Metamorphic Geology*, *18*(1), 67–78.

Platt, J. P. (1986). Dynamics of orogenic wedges and the uplift of high-pressure metamorphic rocks. *Geological Society of America Bulletin*, *97*(9), 1037–1053.

Pleuger, J., & Podladchikov, Y. Y. (2014). A purely structural restoration of the NFP20-East cross section and potential tectonic overpressure in the Adula Nappe (Central Alps). *Tectonics*, *33*, 656–685. https://doi.org/10.1002/2013TC003409

Proyer, A., Dachs, E., & Kurz, W. (1999). Relics of high-pressure metamorphism in the Glockner region, Hohe Tauern, Austria: Textures and mineral chemistry of retrogressed eclogites. *Mitteilungen der Österreichischen Geologischen Gesellschaft*, *90*, 43–55.

Ramberg, H. (1964). Selective buckling of composite layers with contrasted rheological properties, a theory for simultaneous formation of several orders of folds. *Tectonophysics*, *1*(4), 307–341.

Ratschbacher, L., Frisch, W., Linzer, H.-G., & Merle, O. (1991). Lateral extrusion in the Eastern Alps, part 2: Structural analysis. *Tectonics*, *10*(2), 257–271.

Reber, J. E., Dabrowski, M., & Schmid, D. W. (2012). Sheath fold formation around slip surfaces. *Terra Nova*, *24*(5), 417–421.

Rosas, F., Marques, F. O., Luz, A., & Coelho, S. (2002). Sheath folds formed by drag induced by rotation of rigid inclusions in viscous simple shear flow: Nature and experiment. *Journal of Structural Geology*, *24*(1), 45–55.

Rosenberg, C. L., Brun, J.-P., Cagnard, F., & Gapais, D. (2007). Oblique indentation in the Eastern Alps: Insights from laboratory experiments. *Tectonics*, *26*, TC2003. https://doi.org/10.1029/2006TC001960

Rutland, R. W.R. (1965). Tectonic overpressures. Controls of metamorphism, 119–139.

Sander, B. (1914). Geologische studien am Westende der Hohen Tauern. Denkschriften der Kaiserlichen Akademie der Wissenschaften, 82.

Scharf, A., Handy, M. R., Favaro, S., Schmid, S. M., & Bertrand, A. (2013). Modes of orogen-parallel stretching and extensional exhumation in response to microplate indentation and roll-back subduction (Tauern Window, Eastern Alps). *International Journal of Earth Sciences*, *102*(6), 1627–1654.

Scharf, A., Handy, M. R., Ziemann, M. A., & Schmid, S. M. (2013). Peak-temperature patterns of polyphase metamorphism resulting from accretion, subduction and collision (eastern Tauern Window, European Alps)—A study with Raman microspectroscopy on carbonaceous material (RSCM). *Journal of Metamorphic Geology*, *31*(8), 863–880.

Schenker, F. L., Schmalholz, S. M., Moulas, E., Pleuger, J., Baumgartner, L. P., Podladchikov, Y., et al. (2015). Current challenges for explaining (ultra) high-pressure tectonism in the Pennine domain of the Central and Western Alps. *Journal of Metamorphic Geology*, *33*(8), 869–886. https://doi.org/10.1111/jmg.12143

Schmid, S. M., Fügenschuh, B., Kissling, E., & Schuster, R. (2004). Tectonic map and overall architecture of the Alpine orogen. *Eclogae Geologicae Helvetiae*, *97*(1), 93–117.

Schmid, S. M., Pfiffner, O.-A., Froitzheim, N., Schönborn, G., & Kissling, E. (1996). Geophysical-geological transect and tectonic evolution of the Swiss-Italian Alps. *Tectonics*, *15*(5), 1036–1064.

Schmid, S. M., Scharf, A., Handy, M. R., & Rosenberg, C. L. (2013). The Tauern Window (Eastern Alps, Austria): A new tectonic map, with cross-sections and a tectonometamorphic synthesis. *Swiss Journal of Geosciences*, *106*(1), 1–32.

Schmidt, K., Handy, M. R., Scharf, A., Milke, R., John, T., & Oberhänsli, R. (2014). First evidence of subduction-related metamorphism in the most distal European continental margin unit of the Eastern Alps (Modereck Nappe, Tauern Window). In TSK15 Potsdam 2014 Abstract Volume.

Selverstone, J. (1993). Micro- to macroscale interactions between deformational and metamorphic processes, Tauern Window, Eastern Alps. *Schweizerische Mineralogische und Petrographische Mitteilungen*, *73*(2), 229–239.

Selverstone, J., Spear, F. S., Franz, G., & Morteani, G. (1984). High-pressure metamorphism in the SW Tauern Window, Austria: PT paths from hornblende-kyanite-staurolite schists. *Journal of Petrology*, *25*(2), 501–531.

Steck, A., Epard, J.-L., & Masson, H. (2019). The Maggia Nappe: An extruding sheath fold basement nappe in the Lepontine gneiss dome of the Central Alps. *International Journal of Earth Sciences*, *108*(8), 2429–2442.

Tajčmanová, L., Podladchikov, Y., Powell, R., Moulas, E., Vrijmoed, J. C., & Connolly, J. A. D. (2014). Grain-scale pressure variations and chemical equilibrium in high-grade metamorphic rocks. *Journal of Metamorphic Geology*, *32*(2), 195–207.

Vannay, J.-C., & Grasemann, B. (2001). Himalayan inverted metamorphism and syn-convergence extension as a consequence of a general shear extrusion. *Geological Magazine*, *138*(03), 253–276.

Warren, C. J. (2013). Exhumation of (ultra-) high-pressure terranes: Concepts and mechanisms. *Solid Earth*, *4*(1), 75.

Weissert, H. J., & Bernoulli, D. (1985). A transform margin in the Mesozoic Tethys: Evidence from the Swiss Alps. *Geologische Rundschau*, *74*(3), 665–679.

Wheeler, J. (2014). Dramatic effects of stress on metamorphic reactions. *Geology*, *42*(8), 647–650.

Xypolias, P., & Alsop, G. I. (2014). Regional flow perturbation folding within an exhumation channel: A case study from the Cycladic Blueschists. *Journal of Structural Geology*, *62*, 141–155.